AMERICAN SOCIETY FOR MICROBIOLOGY | Infection and Immunity®

CELLULAR MICROBIOLOGY:
PATHOGEN-HOST CELL MOLECULAR INTERACTIONS

Tricellular Tight Junction Protein Tricellulin Is Targeted by the Enteropathogenic *Escherichia coli* Effector EspG1, Leading to Epithelial Barrier Disruption

Vijay Morampudi,[a,b] Franziska A. Graef,[a,b] Martin Stahl,[a,b] Udit Dalwadi,[a,b] Victoria S. Conlin,[a,b] Tina Huang,[a,b] Bruce A. Vallance,[a,b] Hong B. Yu,[a,b] Kevan Jacobson[a,b,c]

Child and Family Research Institute[a] and Division of Gastroenterology,[b] BC Children's Hospital, Vancouver, British Columbia, Canada; Department of Cellular and Physiological Sciences, University of British Columbia, Vancouver, British Columbia, Canada[c]

ABSTRACT Enteropathogenic *Escherichia coli* (EPEC)-induced diarrhea is often associated with disruption of intestinal epithelial tight junctions. Although studies have shown alterations in the expression and localization of bicellular tight junction proteins during EPEC infections, little is known about whether tricellular tight junction proteins (tTJs) are affected. Using Caco-2 cell monolayers, we investigated if EPEC is capable of targeting the tTJ protein tricellulin. Our results demonstrated that at 4 h postinfection, EPEC induced a significant reduction in tricellulin levels, accompanied by a significant loss of transepithelial resistance (TEER) and a corresponding increase in paracellular permeability. Conversely, cells overexpressing tricellulin were highly resistant to EPEC-induced barrier disruption. Confocal microscopy revealed the distribution of tricellulin into the plasma membrane of infected epithelial cells and confirmed the localization of EPEC aggregates in close proximity to tTJs. Moreover, infections with EPEC strains lacking genes encoding specific type III secreted effector proteins demonstrated a crucial role for the effector EspG1 in modulating tricellulin expression. Complementation studies suggest that the EspG-induced depletion of tricellulin is microtubule dependent. Overall, our results show that EPEC-induced epithelial barrier dysfunction is mediated in part by EspG1-induced microtubule-dependent depletion of tricellulin.

KEYWORDS tight junctions, tricellulin, epithelial barrier function, type III secretion system, enteropathogenic *Escherichia coli*, EspG, virulence

Received 10 August 2016 **Returned for modification** 30 August 2016 **Accepted** 16 October 2016

Accepted manuscript posted online 24 October 2016

Citation Morampudi V, Graef FA, Stahl M, Dalwadi U, Conlin VS, Huang T, Vallance BA, Yu HB, Jacobson K. 2017. Tricellular tight junction protein tricellulin is targeted by the enteropathogenic *Escherichia coli* effector EspG1, leading to epithelial barrier disruption. Infect Immun 85:e00700-16. https://doi.org/10.1128/IAI.00700-16.

Editor Andreas J. Bäumler, University of California, Davis

Address correspondence to Kevan Jacobson, kjacobson@cw.bc.ca.

H.B.Y. and K.J. contributed equally to this article.

In the mammalian intestine, tight junction (TJ) proteins located on the apical surface of intestinal epithelial cells (IECs) are crucial for the maintenance of intestinal epithelial barrier integrity (1, 2). Under physiological conditions, TJ proteins help maintain epithelial barrier integrity by controlling the transport of integral membrane proteins and other macromolecules, such as lipids and carbohydrates, from apical to basolateral surfaces (3, 4). Moreover, TJs function as a selective barrier to prevent the passage of microbes and dietary antigens into subepithelial tissues as well as to facilitate the passive transport of water, nutrients, and ions (5, 6). However, under infectious conditions, enteric pathogens, such as enteropathogenic *Escherichia coli* (EPEC), have developed a myriad of ways to disrupt TJ integrity, resulting in the loss of epithelial barrier homeostasis (7–9).

EPEC is an important pathogen that causes diarrhea in young children. Its pathogenicity is mainly mediated through a type III secretion system (T3SS) encoded by a

35-kbp genomic pathogenicity island known as the locus of enterocyte effacement (LEE) (10, 11). EPEC primarily targets IECs, disrupting their function and inducing diarrhea (12, 13). Once EPEC adheres to IECs, the microvilli on the apical surface are effaced from the host cell, forming a characteristic attaching-and-effacing (A/E) lesion. At the site of infection, EPEC intimately attaches to the plasma membrane of the host cell via Tir-intimin interactions, resulting in the formation of an actin-rich pedestal-like structure at the base of the EPEC attachment site (11, 14). Subsequently, type III effector proteins, including EspF, EspG, Map, and EspH, are delivered directly into the host cell cytosol, where they interact with host cellular components. This leads to alterations in cell signaling pathways, resulting in the loss of TJ integrity, mitochondrial dysfunction, and electrolyte imbalances (15–18).

TJs play a crucial role in the maintenance of intestinal paracellular permeability, and their disruption by EPEC has been associated with the loss of the epithelial barrier function. Depending upon the location on the surface of epithelial cells, TJ proteins can be classified into two groups: bicellular tight junction (bTJ) proteins, located at the junction between two adjacent cells, and tricellular tight junction (tTJ) proteins, typically located between three or four cells. However, unlike tTJ proteins, bTJ proteins, including occludin and claudins (1–24) as well as other TJ-associated proteins, such as ZO-1, ZO-2, and ZO-3, have been well studied. Tricellulin, a 64-kDa transmembrane protein, was the first protein to be identified to be exclusively located at tTJs (19, 20). Tricellulin consists of four transmembrane domains, with both the amino and carboxy termini being located inside the cytoplasm of cells. Interestingly, tricellulin was shown to be structurally related to the bTJ protein occludin and shares a conserved ~130-amino-acid carboxy-terminal sequence with occludin, suggesting that they are paralogues of each other resulting from gene duplication (19). Mutations in the tricellulin gene (DFNB49) were found to be associated with nonsyndromic deafness in humans (21). Further, studies using small interfering RNA (siRNA) to deplete tricellulin expression have demonstrated impaired epithelial barrier resistance, along with increased permeability (19). Consistent with this notion, the level of tricellulin expression was noted to be very low in gut tissues from patients with inflammatory bowel disease (IBD), whose intestinal epithelium is often compromised (22). More recently, tricellulin was shown to promote the dissemination of the intracellular pathogen *Shigella* from one epithelial cell to another, thus implicating tricellulin as an unexpected target during enteric bacterial infections (23).

We and others have shown that EPEC-induced epithelial barrier disruption occurs via the redistribution and reorganization of bTJ proteins, such as occludin, ZO-1, and claudins 1, 4, and 5 (12, 24, 25), thereby causing overt changes in IEC function. However, it remains unclear whether tTJ proteins also serve as a target for EPEC infection and whether such targeting leads to epithelial barrier disruption (16, 26). Based on its apical location and functional role in the maintenance of barrier integrity, we hypothesized that EPEC might exploit tricellulin by altering its expression and/or distribution during infection. We showed that during the course of EPEC infection, tricellulin expression was significantly downregulated and was associated with a significant decrease in transepithelial resistance (TEER) and an increase in barrier permeability. We demonstrated a selective role for the type III secreted effector EspG1 in downregulating tricellulin expression via the disruption of microtubule filaments. This research highlights a key role for tricellulin in epithelial barrier integrity and demonstrates that EPEC-induced barrier disruption is in part mediated through disruption of tricellulin homeostasis. Moreover, this study suggests that tricellulin may serve as a potential therapeutic target to impede EPEC-induced barrier disruption.

RESULTS

Infection of IEC with EPEC but not AIEC significantly reduces tricellulin expression. Previous studies with the enteric pathogen *Shigella* demonstrated a crucial role for tricellulin in mediating the spread of *Shigella* between epithelial cells (23). We hypothesized that tricellulin can be targeted by other enteric pathogens, such as

adherent-invasive *E. coli* (AIEC) and enteropathogenic *E. coli* (EPEC). To test this possibility, Caco-2 cells grown on Transwells were infected for 4 h with either invasive AIEC pathogens or attaching-and-effacing EPEC pathogens. We then studied the epithelial barrier function by measuring TEER and the level of fluorescein isothiocyanate (FITC)-dextran fluorescence as markers to analyze epithelial barrier resistance and permeability, respectively. Compared to the uninfected controls, both AIEC- and EPEC-infected cells demonstrated a reduction in TEER (Fig. 1A); however, the decline in TEER was significant only in EPEC-infected cells. Consistent with the time-dependent decrease in TEER, a corresponding increase in barrier permeability was observed at between 2 h and 4 h in EPEC-infected cells (Fig. 1B). The permeability of AIEC-infected cells was not altered (Fig. 1B).

Since TJ proteins are often compromised during enteric infections, we next probed for changes in the levels of expression of the genes for the bi- and tricellular junction proteins occludin, claudin-1, and tricellulin. Although no significant differences in the transcript levels of claudin-1 and occludin were observed, a significant reduction in tricellulin transcript levels was noted in EPEC-infected cells but not in AIEC-infected cells (Fig. 1C). Furthermore, immunoblotting of whole-cell lysates confirmed a reduction in the levels of tricellulin expression in EPEC-infected cells at 4 h postinfection (p.i.). (Fig. 1D). To test whether the loss of tricellulin directly reduced barrier resistance and increased permeability, tricellulin knockdown experiments were performed using siRNA (200 nM and 400 nM). As shown in Fig. 1E and F, a striking decrease in resistance with a corresponding increase in barrier permeability was observed in Caco-2 cells transfected with tricellulin-specific siRNA compared to the findings for cells transfected with control siRNA, similar to what was previously reported for tricellulin knockdown in EpH4 cells (19). Immunoblotting analysis and the corresponding semiquantitative band density analysis confirmed that the tricellulin-specific siRNA treatment specifically depleted tricellulin but not claudin-3, used as a negative control to evaluate siRNA specificity (Fig. 1G). Thus, EPEC infection significantly impairs intestinal epithelial barrier resistance, increases permeability, and is accompanied by a decrease in the level of expression of the tTJ protein tricellulin.

EPEC-induced changes in tricellulin expression/distribution are dependent on the functional T3SS. Based on the marked decrease in tricellulin expression observed during EPEC infection, we next analyzed whether the EPEC T3SS is required to modulate tricellulin expression. We first infected cells with a Δ*escN* mutant which lacks the ATPase required for the proper function of the T3SS. As shown in Fig. 2A, cells infected with the Δ*escN* mutant demonstrated TEER values comparable to those seen in uninfected cells over the 4-h infection period (Fig. 2A). Moreover, Δ*escN* mutant-infected cells maintained 52% and 82% higher TEER values than wild-type (WT) EPEC-infected cells at 3 h and 4 h p.i., respectively. In addition, an 85% decrease in the level of permeation of the FITC-dextran tracer was observed in Δ*escN* mutant-infected cells than WT EPEC-infected cells at 4 h p.i. (Fig. 2B). Of note, when the cell lysates were probed for tricellulin expression, stronger signals were observed in Δ*escN* mutant-infected cells than WT EPEC-infected cells, suggesting a key role for EPEC's T3SS in modulating tricellulin expression (Fig. 2C).

To further investigate if the loss of barrier function during WT EPEC infection is accompanied by alterations in tricellulin localization and whether this was T3SS dependent, immunostaining of paraformaldehyde (PFA)-fixed Caco-2 cells was performed. Fluorescence microscopy of noninfected cells revealed (as expected) the localization of tricellulin strictly restricted to tTJs (Fig. 2D). However, in cells infected with WT EPEC, tricellulin began to lose its native dot-like structure and appeared to be elongated and distributed randomly near tTJs (Fig. 2D). In contrast, the level of tricellulin expression and tricellulin localization in Δ*escN* mutant-infected cells closely resembled those observed in uninfected cells (Fig. 2D). Quantitative analysis of the total number of tricellulin-positive dot-like structures present at the tTJs demonstrated significantly fewer in EPEC-infected cells than control or Δ*escN* mutant-infected cells (Fig. 2E). To examine if EPEC is localized near tTJs during infection, confocal imaging was performed

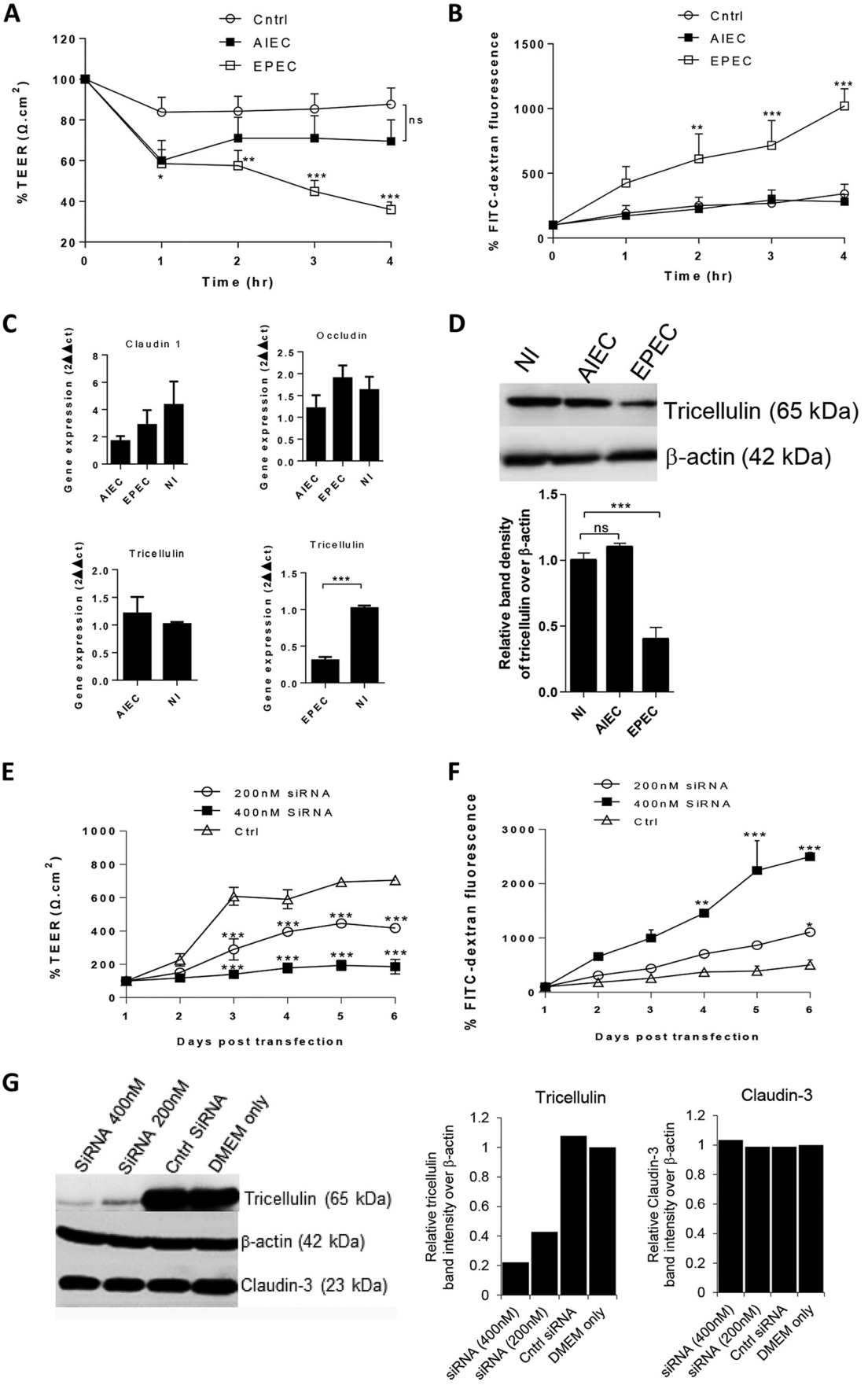
A
Cntrl
AIEC
EPEC
% TEER (Ω.cm 2)
Time (hr)
ns
B
% FITC-dextran fluorescence
Time (hr)
C
Claudin 1
Occludin
Tricellulin
Gene expression (2▲▲ct)
AIEC
EPEC
NI
D
NI
AIEC
EPEC
Tricellulin (65 kDa)
β-actin (42 kDa)
Relative band density of tricellulin over β-actin
E
200nM siRNA
400nM SiRNA
Ctrl
% TEER (Ω.cm 2)
Days post transfection
F
% FITC-dextran fluorescence
Days post transfection
G
SiRNA 400nM
SiRNA 200nM
Cntrl SiRNA
DMEM only
Tricellulin (65 kDa)
β-actin (42 kDa)
Claudin-3 (23 kDa)
Tricellulin
Claudin-3
Relative tricellulin band intensity over β-actin
Relative Claudin-3 band intensity over β-actin
siRNA (400nM)
siRNA (200nM)
Cntrl siRNA
DMEM only

on cells infected with green fluorescent protein (GFP)-labeled WT EPEC. Although we observed EPEC bacteria distributed all over the epithelial cell surface, microcolonies were detected in close proximity to tTJs (Fig. 2F). We also noted that tricellulin was often distributed along the bTJs, rather than being localized to the tTJ. Interestingly, the mislocalization of tricellulin to bTJs has previously been reported in occludin-deficient Madin-Darby canine kidney (MDCK) cells and lipolysis-stimulated lipoprotein receptor knockout EpH4 epithelial cells (27, 28). In contrast, when cells were infected with GFP-labeled Δ*escN* strains, the bacteria lost their ability to form microcolonies, were unable to localize near tTJs, and were found to be unevenly spread across the surface of cells (Fig. 2F). Overall, these results suggest an important role for EPEC's T3SS in its ability to alter tricellulin expression and distribution.

Type III secreted effectors EspF, Map, and EspH are not required for tricellulin disruption by EPEC. To identify potential type III secreted effectors that target tricellulin, EPEC strains lacking effectors known to disrupt TJ proteins (EspF and Map) or promote pedestal formation (EspH) were used for subsequent analysis (18, 29, 30). To test the role of these effectors in altering the epithelial barrier function, Caco-2 cells were infected with the mutant strains. As shown in Fig. 3A, Caco-2 cells infected with the Δ*espF* mutant demonstrated resistance values that fell between those of control cells and WT EPEC-infected cells. Although there was a moderate increase in the level of resistance from 1 h to 2 h p.i., a consistent decline was observed from 2 h to 4 h p.i. in Δ*espF* mutant-infected cells (Fig. 3B). At 4 h p.i., no significant difference in TEER values was observed between Δ*espF* mutant-infected cells and WT EPEC-infected cells. A modest but nonsignificant increase in FITC-dextran tracer fluorescence across Caco-2 cells was also observed following Δ*espF* mutant infection (Fig. 3A and B). Infections with the Δ*map* EPEC strain resulted in a significant 33% and 48% decrease in resistance at 3 h and 4 h p.i., respectively, compared to that in control cells, reaching levels similar to those seen with WT EPEC (Fig. 3A). Increased barrier permeability was also seen in Δ*map* mutant-infected cells, although the difference in FITC-dextran levels compared to the levels in control cells did not reach statistical significance (Fig. 3B). In addition, compared with control cells, infection with the Δ*espH* mutant resulted in a significant 55% and 48% decrease in TEER values at 2 h and 4 h p.i., respectively (Fig. 3A). A significant 146% increase in the level of the FITC-dextran tracer was also seen in Δ*espH* mutant-infected cells, which is again similar to the effects of WT EPEC infection (Fig. 3B). To study whether the effector EspF, Map, or EspH modulated tricellulin expression, lysates from cells infected with the respective mutant EPEC strains were subjected to Western blotting. Similar to the dramatic reduction in tricellulin band intensity (from the levels for lysates from uninfected cells) seen following infection with WT EPEC, lysates collected from cells infected by Δ*espF*, Δ*map*, and Δ*espH* mutant strains demonstrated minimal band intensities for tricellulin, suggesting no overt role for these virulence factors in regulating tricellulin expression (Fig. 3C).

EPEC-induced tricellulin reduction is partially dependent on EspG. The T3SS effector EspG has been shown to be crucial in EPEC's ability to alter epithelial barrier permeability by activating the RhoA signaling pathway (31). EPEC produces 2 versions of EspG-EspG1 which are encoded within the LEE, while the region encoding its homolog, EspG2, is located in the EspC pathogenicity island (32). To elucidate the function of EspG1 and/or EspG2 in modulating tricellulin expression, we infected Caco-2 cell monolayers with a single mutant strain (the Δ*espG1* mutant) or a double

FIG 1 Significant reduction of tricellulin expression in IECs infected with EPEC. (A and B) Caco-2 cells infected with AIEC or EPEC were measured for TEER (A) and FITC-dextran tracer fluorescence (B). (C) AIEC- and EPEC-infected cells were evaluated for the transcription of TJ proteins claudin-1, occludin, and tricellulin. (D) AIEC and EPEC cell lysates were probed for tricellulin expression at 4 h p.i. (E and F) Cells transfected with tricellulin-specific siRNA were measured for changes in TEER (E) and FITC-dextran tracer fluorescence (F). (G) Cell lysates from siRNA-transfected cells were probed for the expression of tricellulin and claudin-3 expression (left), and their corresponding band densities relative to the density for β-actin were plotted (right). The TEER and FITC fluorescence data shown in panels A, B, E, and F are averages from 3 independent experiments with 3 wells per condition. For semiquantitative bar graph analysis of the Western blots, 3 independent experiments with a total of 2 wells per condition were used. *, $P < 0.01$; **, $P < 0.001$; ***, $P < 0.0001$; ns, nonsignificant. Cntrl and Ctrl, control; NI, noninfected controls.

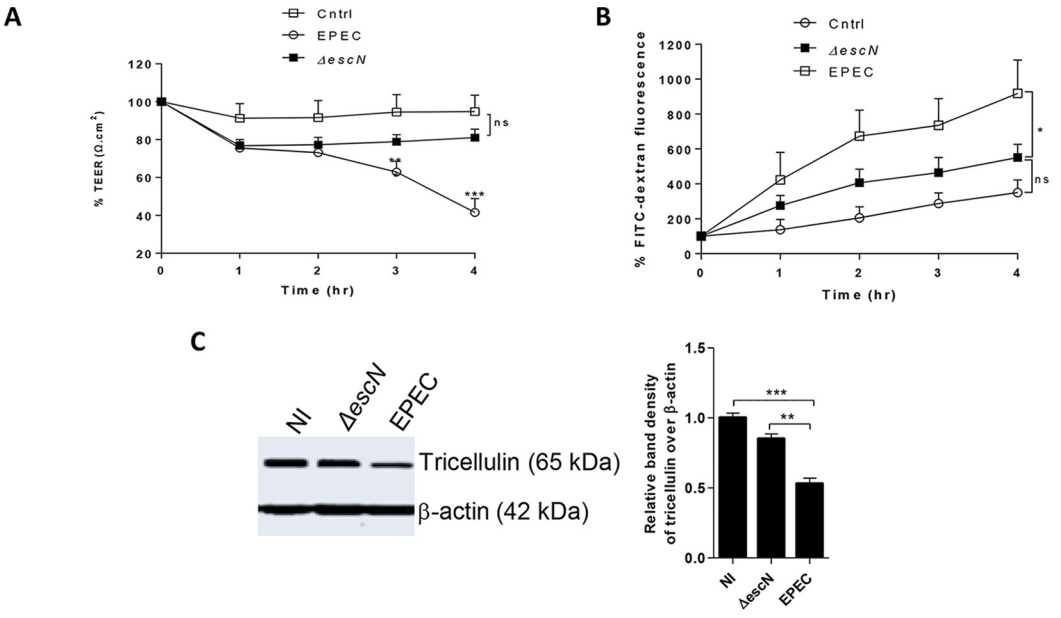
A
Cntrl
EPEC
ΔescN
% TEER (Ω.cm²)
Time (hr)
ns
**
***
B
Cntrl
ΔescN
EPEC
% FITC-dextran fluorescence
Time (hr)
*
ns
C
NI
ΔescN
EPEC
Tricellulin (65 kDa)
β-actin (42 kDa)
Relative band density of tricellulin over β-actin
***
**
NI
ΔescN
EPEC

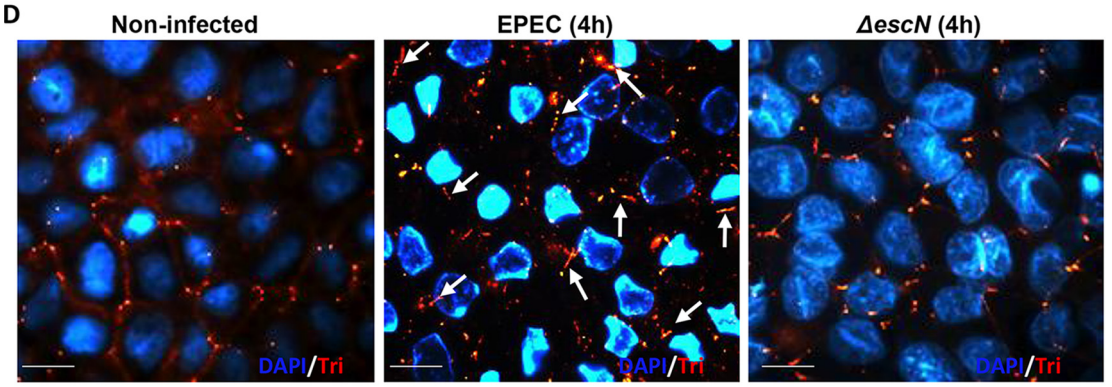
D
Non-infected
EPEC (4h)
ΔescN (4h)
DAPI/Tri
DAPI/Tri
DAPI/Tri

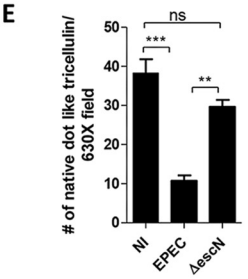
E
# of native dot like tricellulin/ 630X field
ns
***
**
NI
EPEC
ΔescN

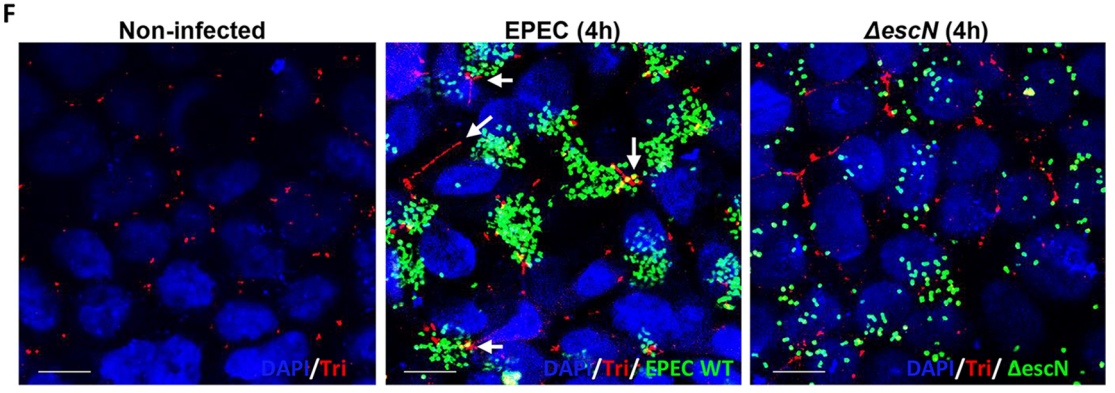
F
Non-infected
EPEC (4h)
ΔescN (4h)
DAPI/Tri
DAPI/Tri/EPEC WT
DAPI/Tri/ ΔescN

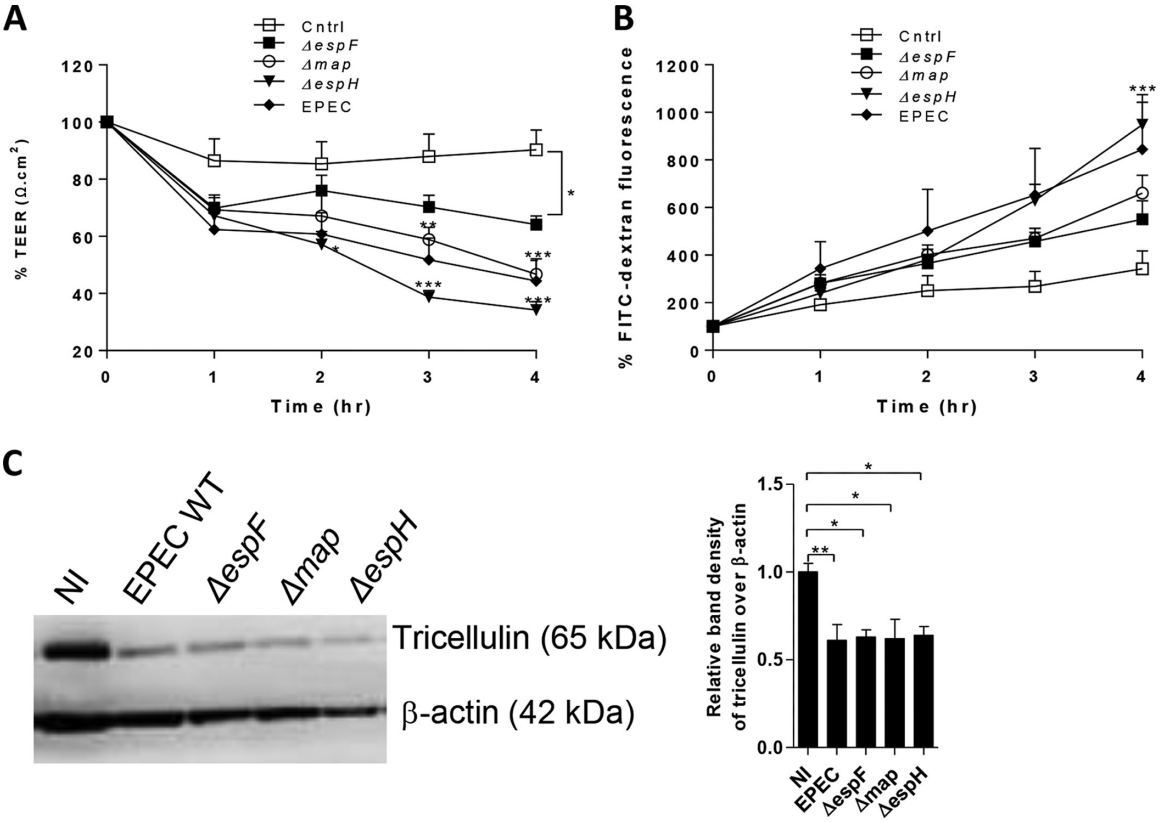

FIG 3 Reduced tricellulin expression is independent of *espF*, *map*, and *espH*. (A and B) Caco-2 cells infected with Δ*espF*, Δ*map*, and Δ*espH* mutant strains were measured for TEER (A) and FITC-dextran tracer fluorescence (B). The TEER and FITC fluorescence data are representative of those from an average of >3 independent experiments with 3 wells per condition. (C) Tricellulin protein expression on lysates obtained from cells infected with mutant Δ*espF*, Δ*map*, and Δ*espH* strains. For Western blot analysis, 3 independent experiments with 2 wells per condition were used. *, $P < 0.01$; **, $P < 0.001$; ***, $P < 0.0001$.

mutant strain (the Δ*espG1* Δ*espG2* mutant). In contrast to WT EPEC-infected cells, both the single and double *espG* mutant strains were associated with an attenuated reduction in the drop in epithelial resistance during the course of 4 h of infection ($P < 0.0001$ for the Δ*espG1* mutant and $P < 0.0001$ for the Δ*espG1* Δ*espG2* mutant) (Fig. 4A). In line with this result, cells infected with the Δ*espG1* and Δ*espG1* Δ*espG2* mutants demonstrated FITC-dextran tracer levels similar to those seen in uninfected cells. Thus, EspG1 plays a critical role in promoting barrier disruption during EPEC infection (Fig. 4B).

To elucidate whether EspG1 plays a role in modulating tricellulin expression, immunoblotting of cell lysates obtained at 4 h p.i. was performed. As shown in Fig. 4C, only minimal changes in tricellulin expression were seen in lysates from Δ*espG1* and Δ*espG1* Δ*espG2* mutant-infected cells, in contrast to the considerable loss of tricellulin observed in WT EPEC-infected cells (0.91 ± 0.06 for the Δ*espG1* mutant, 0.73 ± 0.05 for the Δ*espG1* Δ*espG2* mutant, and 0.38 ± 0.09 for the WT EPEC strain) (Fig. 4C). Such differences in tricellulin expression were not due to the overall defects in the colonization of different *espG* mutant strains since the extent to which the WT, Δ*espG1*

FIG 2 Tricellulin expression and localization to tTJs are dependent on EPEC T3SS. (A and B) Caco-2 cells were infected with Δ*escN* mutant EPEC strains and measured for TEER (A) and FITC-dextran tracer fluorescence (B). The data are averages from >3 independent experiments with 3 wells per condition. Two independent experiments with 3 wells per condition were used for analysis. (C) Cell lysates obtained from control, Δ*escN* mutant, and WT EPEC strains were probed for the expression of tricellulin. (D) Tricellulin (Tri) detection by fluorescence microscopy in noninfected, Δ*escN* mutant-infected, and WT EPEC-infected cells. Magnifications, ×2,000. (E) Microscopic evaluation of the total number of native dot-like tricellulin structures localized at tTJs. For each strain, a minimum of 8 to 10 images from 3 independent experiments were analyzed at a magnification of ×630. (F) Confocal imaging of cells infected with GFP-labeled WT EPEC and Δ*escN* EPEC strains immunolabeled for tricellulin. Magnifications, ×2,000. For panels D and F, blue, nuclei; green, GFP-labeled EPEC; red, tricellulin. *, $P < 0.01$; **, $P < 0.001$; ***, $P < 0.0001$; ns, nonsignificant. Arrows, loss of native dot-like structure of tricellulin.

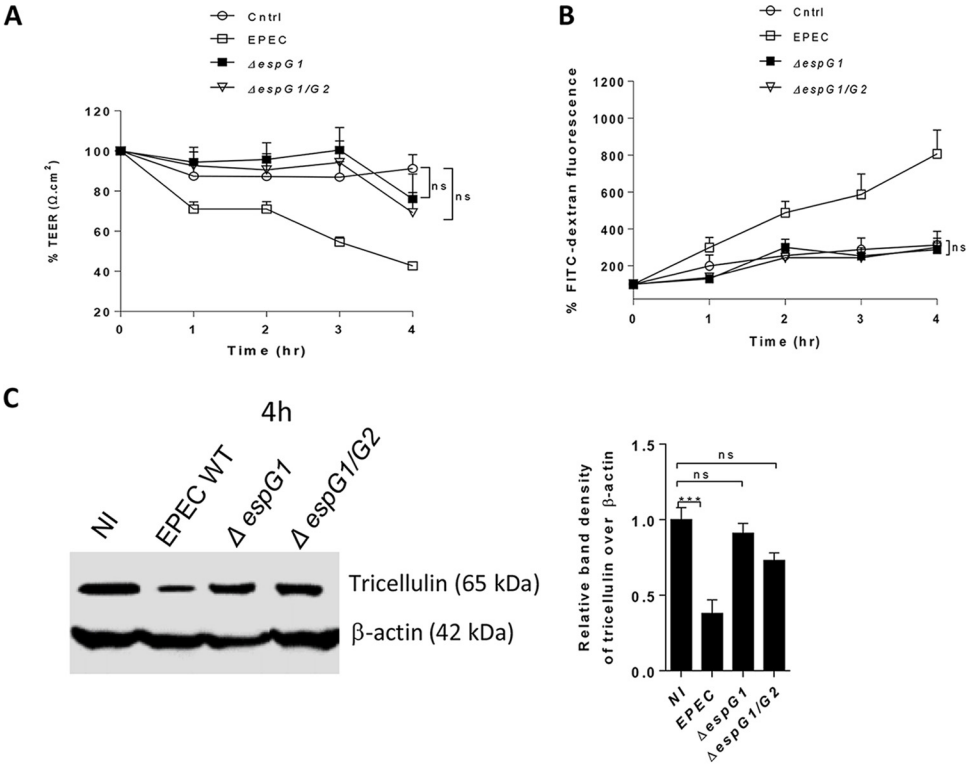
A
Cntrl
EPEC
ΔespG1
ΔespG1/G2
% TEER (Ω.cm²)
Time (hr)
ns
ns
B
% FITC-dextran fluorescence
Time (hr)
ns
C
4h
NI
EPEC WT
Δ espG1
Δ espG1/G2
Tricellulin (65 kDa)
β-actin (42 kDa)
Relative band density of tricellulin over β-actin
***
ns
ns
NI
EPEC
ΔespG1
ΔespG1/G2

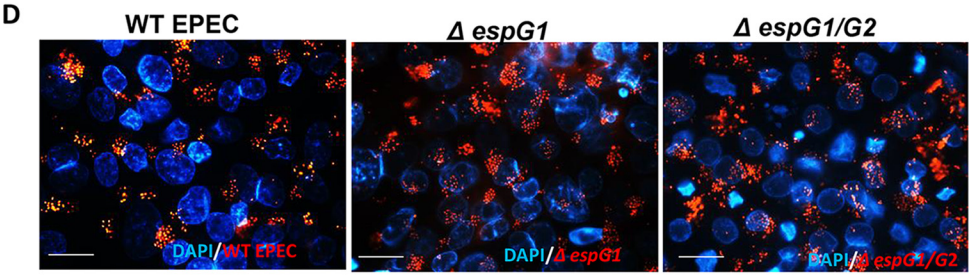
D
WT EPEC
Δ espG1
Δ espG1/G2
DAPI/WT EPEC
DAPI/Δ espG1
DAPI/Δ espG1/G2

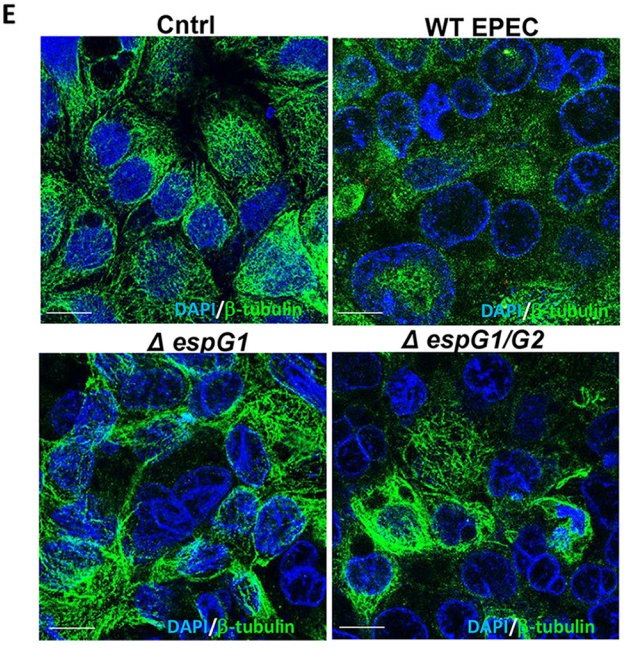
E
Cntrl
WT EPEC
Δ espG1
Δ espG1/G2
DAPI/β-tubulin
DAPI/β-tubulin
DAPI/β-tubulin
DAPI/β-tubulin

mutant, and Δ*espG1* Δ*espG2* mutant microcolonies formed near tTJs at 4 h p.i. was comparable (Fig. 4D). Furthermore, WT EPEC and both *espG* mutant strains demonstrated similar growth rates and cell adherence capabilities (data not shown). These results suggest that the effector EspG1 plays a major role in the depletion of tricellulin during EPEC infection.

Previous studies suggested that EspG causes barrier disruption by targeting intracellular microtubules (13, 33). Consistent with the findings of these studies, confocal imaging analysis revealed that the WT EPEC strain but not the Δ*espG1* or Δ*espG1* Δ*espG2* strain induced a significant loss of microtubule structures (Fig. 4E). So far, these results identify EspG1 to be one of the key T3SS effectors that induces the loss of barrier function along with a significant disruption of microtubules and a reduction in the level of tricellulin expression.

Complementation with FL EspG1 restores changes in tricellulin expression. To confirm that EspG1 indeed plays a crucial role in modulating the epithelial barrier function as well as tricellulin expression, we infected cells with Δ*espG1* and Δ*espG1* Δ*espG2* strains transformed with a plasmid expressing full-length (FL) EspG1 (the Δ*espG1* mutant-FL and Δ*espG1* Δ*espG2* mutant-FL strains, respectively). Δ*espG1* mutant-FL-infected cells demonstrated a greater decrease in resistance values than Δ*espG1* mutant-infected cells at all time points (with a significant 35% decrease being observed at the 4-h time point) (Fig. 5A). A striking 246% increase in FITC-dextran translocation was also observed in Δ*espG1* mutant-FL-infected cells in comparison to cells infected with Δ*espG1* mutant EPEC (Fig. 5B). Moreover, compared to Δ*espG1* Δ*espG2* mutant-infected cells, a significant 42% reduction in resistance and a 142% increase in FITC-dextran permeability were observed at 4 h p.i. in cells infected with Δ*espG1* Δ*espG2* mutant-FL (Fig. 5A and B). In line with the results presented above, immunoblotting of cell lysates obtained from Δ*espG1* mutant-FL- and Δ*espG1* Δ*espG2* mutant-FL-infected cells showed a dramatic reduction in the levels of tricellulin expression similar to those observed in lysates from WT EPEC-infected cells (0.24 ± 0.01 in Δ*espG1* mutant-FL-infected cells, 0.16 ± 0.07 in Δ*espG1* Δ*espG2* mutant-FL-infected cells, and 0.33 ± 0.09 in WT EPEC-infected cells) (Fig. 5C). Taken together, these results confirm that EspG1 is one of the key type III secreted effectors that induces the loss of the epithelial barrier function, likely via disruption of tricellulin expression. Whether EspG2 also contributes to tricellulin disruption will be addressed in future studies.

EspG1-induced tricellulin disruption is microtubule dependent. One of the mechanisms by which EspG disrupts the epithelial barrier function is through depolymerization of intracellular microtubules (13, 32–34). Hence, we were interested in examining if EspG-induced microtubule disruption plays a role in modulating tricellulin expression. To address this, we first infected Caco2 cells with the Δ*espG1* mutant-FL-ΔTB and Δ*espG1* Δ*espG2* mutant-FL-ΔTB strains (constructed by using the Δ*espG1* and Δ*espG1* Δ*espG2* strains transformed with a plasmid expressing FL-ΔTB). FL-ΔTB is a truncated version of EspG1 that lacks a putative tubulin binding (TB) domain from V220 to Q332 (34). We reasoned that deletion of this putative TB domain would render EspG1 incapable of causing microtubule disruption. Indeed, confocal imaging analysis revealed a significant reduction in microtubule disruption in Caco-2 cells infected with Δ*espG1* mutant-FL-ΔTB and Δ*espG1* Δ*espG2* mutant-FL-ΔTB at 4 h p.i. compared to that in Δ*espG1* mutant-FL- and Δ*espG1* Δ*espG2* mutant-FL-infected cells (Fig. 6A). Moreover, at 3 h and 4 h p.i., cells infected with the Δ*espG1* mutant-FL-ΔTB strain displayed significantly less of a decrease in resistance (67% and 121%, respectively) in comparison

FIG 4 Tricellulin expression is largely dependent on EspG1. Caco-2 cells infected with WT EPEC, the Δ*espG1* single mutant strain, or the Δ*espG1* Δ*espG2* double EPEC mutant strain (Δ*espG1/G2*) were measured for TEER (A) and FITC-dextran tracer fluorescence (B). The TEER and FITC fluorescence data are averages from >3 independent experiments with 3 wells per condition. (C) WT and mutant EPEC-infected cell lysates were probed for tricellulin expression. (D) Fluorescence microscopy of cells infected with GFP-labeled WT EPEC, Δ*espG1* mutant, and Δ*espG1* Δ*espG2* mutant strains. Magnifications, ×1,000. (E) Confocal imaging of β-tubulin and nuclei (DAPI) on Caco-2 cells infected with WT EPEC, Δ*espG* mutant, and Δ*espG1* Δ*espG2* mutant strains for 4 h. Magnification, ×2,000. For panels D and E, blue, nuclei; green, β-tubulin; red, GFP-labeled WT and mutant EPEC strains. For Western blot analysis, a minimum of 3 independent experiments with 2 or 3 wells per condition were used. ***, $P < 0.0001$; ns, nonsignificant.

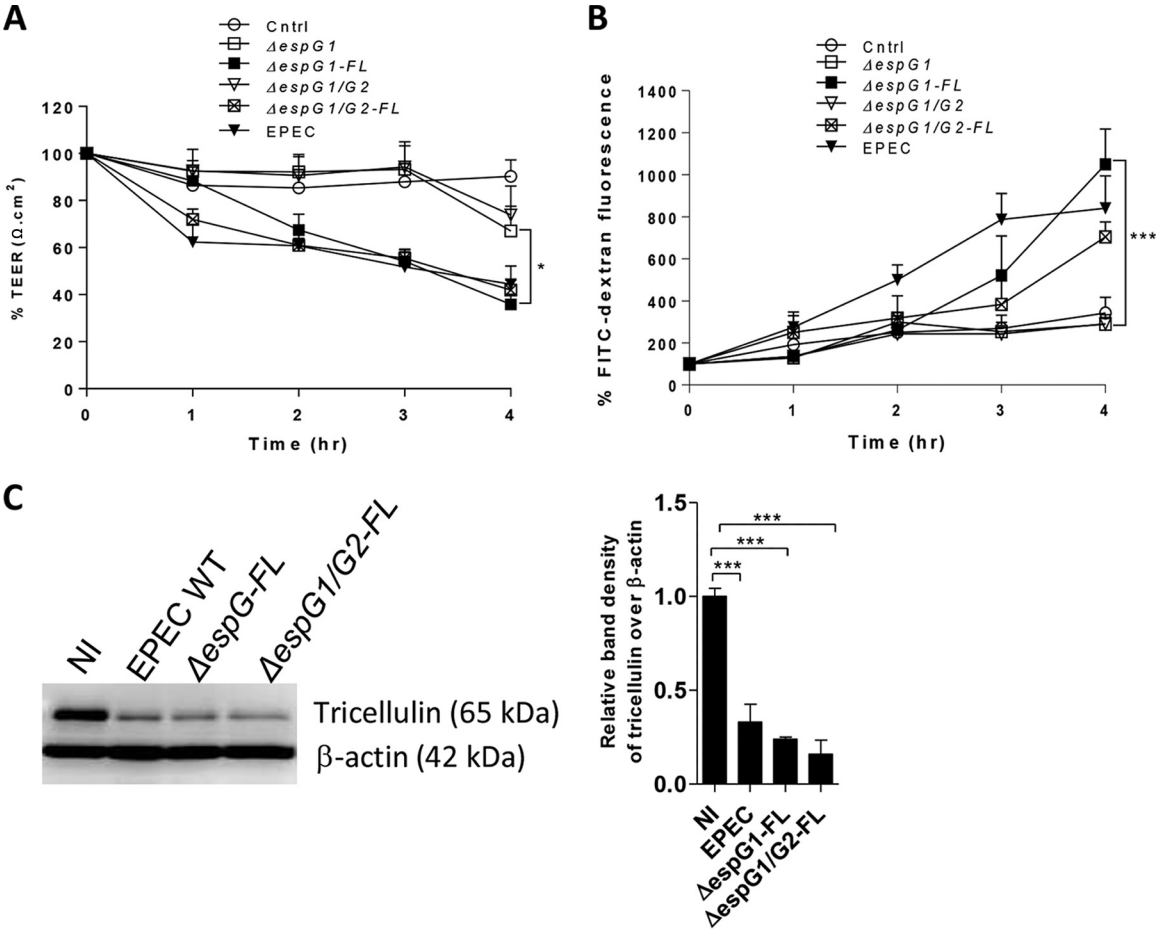

FIG 5 Introducing full-length *espG* into Δ*espG1* and Δ*espG1* Δ*espG2* mutant strains restores the EPEC phenotype. (A and B) Caco-2 cells infected with Δ*espG1* and Δ*espG1* Δ*espG2* mutant strains complemented with full-length *espG*, the Δ*espG1* mutant-FL (Δ*espG1*-FL) and Δ*espG1* Δ*espG2* mutant-FL (Δ*espG1/G2*-FL) strains, were measured for TEER (A) and FITC-dextran tracer fluorescence (B). The FITC fluorescence and TEER data are mean ± SEM values obtained from 3 independent experiments with 3 wells per condition. (C) Cell lysates infected with *espG* mutant strains were probed for tricellulin expression. A minimum of 3 independent experiments with 2 to 3 wells per condition were used for bar graph analysis of the Western blots. *, $P < 0.01$; ***, $P < 0.0001$.

to that in Δ*espG1* mutant-FL-infected cells (Fig. 6B). A significant 290% decrease in FITC-dextran levels was also observed at 4 h p.i. in Δ*espG1* mutant-FL-ΔTB-infected cells in comparison to that in Δ*espG1* mutant-FL-infected cells (Fig. 6C). Interestingly, cells infected with the Δ*espG1* Δ*espG2* mutant-FL-ΔTB strain showed levels of resistance and FITC-dextran levels similar to those in cells infected with the Δ*espG1* mutant-FL-ΔTB strain (Fig. 6B to E) throughout the course of infection. These data not only confirm that EspG1-induced microtubule disruption is associated with barrier disruption (33) but also suggest that the putative TB domain plays a key role in such a process.

Capitalizing on the result described above, we next sought to determine if tricellulin expression is modulated by EspG-induced microtubule disruption. Lysates obtained from cells infected with different EPEC strains were therefore probed for tricellulin expression. As shown in Fig. 6F, in comparison to uninfected cells, tricellulin expression was well maintained in cells infected with the Δ*espG1* mutant-FL-ΔTB and Δ*espG1* Δ*espG2* mutant-FL-ΔTB strains, whereas the level of expression was reduced in Δ*espG1* mutant-FL- and Δ*espG1* Δ*espG2* mutant-FL-infected cells, similar to the loss seen in cells infected with WT EPEC. To further demonstrate if microtubule disruption is associated with an increased loss of tricellulin at tTJs, we also performed fluorescence microscopy of cells infected with the *espG* mutant strains described above. As shown in Fig. 6G, infection with the Δ*espG1* mutant-FL and Δ*espG1* Δ*espG2* mutant-FL strains resulted in the loss of intact tricellulin at tTJs, similar to that observed in WT EPEC, whereas its

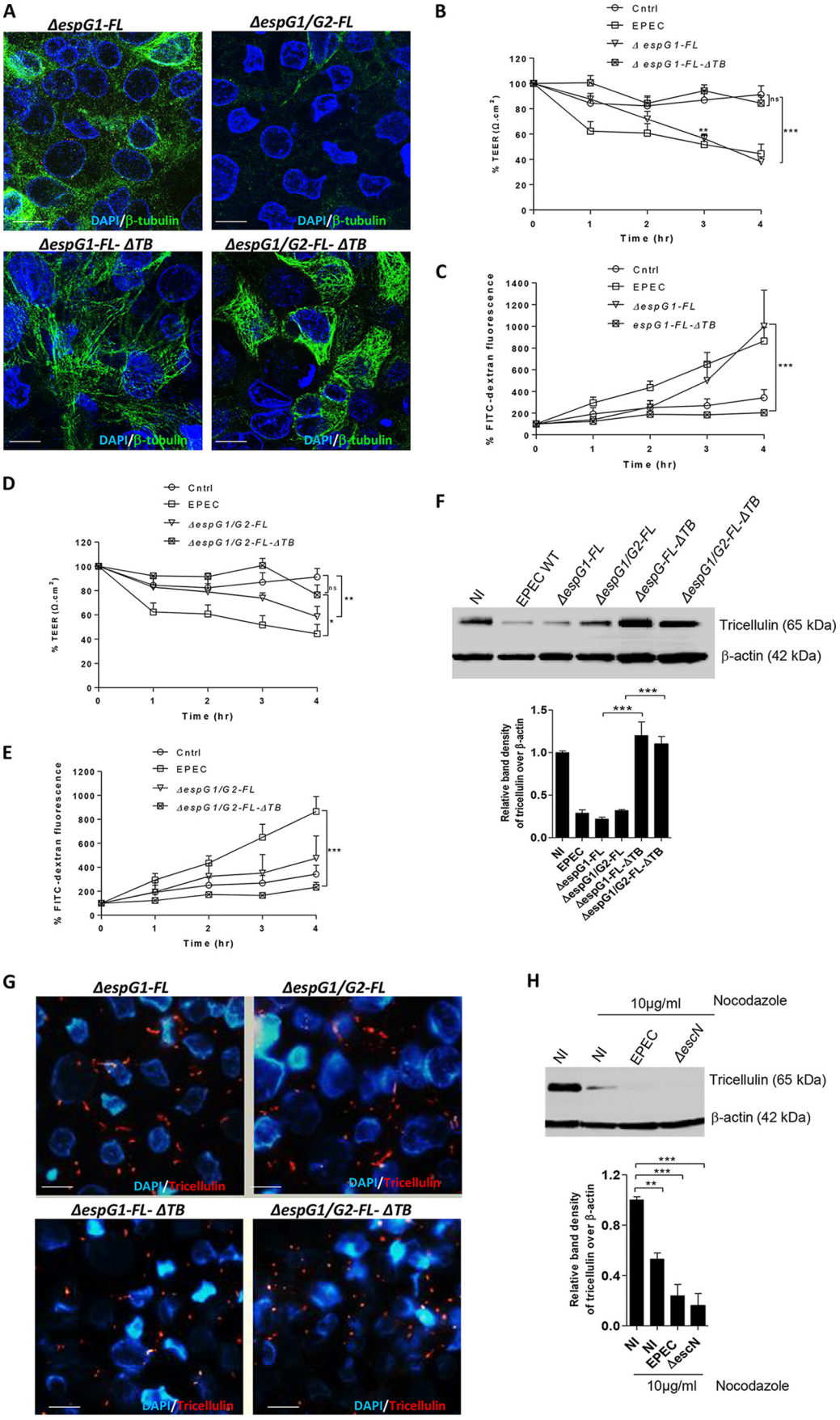
A
ΔespG1-FL
ΔespG1/G2-FL
ΔespG1-FL- ΔTB
ΔespG1/G2-FL- ΔTB
DAPI/β-tubulin
B
Cntrl
EPEC
Δ espG1-FL
Δ espG1-FL-ΔTB
% TEER (Ω.cm²)
Time (hr)
ns
**
***
C
Cntrl
EPEC
ΔespG1-FL
espG1-FL-ΔTB
% FITC-dextran fluorescence
Time (hr)
***
D
Cntrl
EPEC
ΔespG1/G2-FL
ΔespG1/G2-FL-ΔTB
% TEER (Ω.cm²)
Time (hr)
ns
**
*
E
Cntrl
EPEC
ΔespG1/G2-FL
ΔespG1/G2-FL-ΔTB
% FITC-dextran fluorescence
Time (hr)
***
F
NI
EPEC WT
ΔespG1-FL
ΔespG1/G2-FL
ΔespG-FL-ΔTB
ΔespG1/G2-FL-ΔTB
Tricellulin (65 kDa)
β-actin (42 kDa)
Relative band density of tricellulin over β-actin
***
***
NI
EPEC
ΔespG1-FL
ΔespG1/G2-FL
ΔespG1-FL-ΔTB
ΔespG1/G2-FL-ΔTB
G
ΔespG1-FL
ΔespG1/G2-FL
ΔespG1-FL- ΔTB
ΔespG1/G2-FL- ΔTB
DAPI/Tricellulin
H
10μg/ml Nocodazole
NI
NI
EPEC
ΔescN
Tricellulin (65 kDa)
β-actin (42 kDa)
Relative band density of tricellulin over β-actin
***
***
**
NI
NI
EPEC
ΔescN
10μg/ml Nocodazole

structure and localization were well preserved in cells infected with the Δ*espG1* mutant-FL-ΔTB and Δ*espG1* Δ*espG2* mutant-FL-ΔTB strains. Lastly, we tested if microtubule integrity affects tricellulin expression through a chemical approach. Cells were treated with nocodazole, a drug known to disrupt microtubule polymerization, and were left uninfected or were infected with the WT EPEC and Δ*escN* strains. We found that both uninfected and infected cells treated with 10 μg/ml nocodazole showed significantly reduced tricellulin expression. Taken together, the data obtained through both genetic and chemical approaches suggest that disruption of microtubules via EPEC leads to the downregulation of tricellulin (Fig. 6H).

Overexpression of tricellulin increases resistance and modulates EPEC-induced barrier disruption. Since the reduced tricellulin expression was accompanied by significant barrier disruption in both tricellulin-specific siRNA-treated cells and EPEC-infected cells, we hypothesized that the overexpression of tricellulin in Caco-2 cells would enhance the intestinal epithelial barrier function. To test this possibility, we generated a stable Caco-2 cell line that overexpresses tricellulin (Tric-Caco2). We initially determined the impact of tricellulin overexpression alone on TEER measurements. As shown in Fig. 7A, the TEER readings from Tric-Caco2 cells closely resembled those from normal Caco-2 cells until day 16. However, from day 16 to day 20, Tric-Caco-2 cells demonstrated a significant 39.3% to 53% increase in resistance over that seen in Caco-2 cells. To confirm the extent of tricellulin expression at tTJs, Tric-Caco2 cells grown for 20 days were immunostained for tricellulin expression. As expected, an increase in tricellulin staining, which was restricted to tTJs, was observed in Tric-Caco2 cells compared to normal Caco-2 cells (Fig. 7B). Quantitative analysis also revealed an increase in the total number of tricellulin-positive dot-like structures present at the tTJs in Tric-Caco2 cells in comparison to Caco2 cells (Fig. 7C). Immunoblotting of cell lysates also confirmed an increase in tricellulin expression in Tric-Caco2 cells compared to control Caco-2 cells (Fig. 7D). We next examined whether tricellulin overexpression could modulate the intestinal epithelial barrier function during EPEC infection. Tric-Caco2 cells and Caco-2 cells grown for 20 days postseeding were infected with EPEC for 4 h. Compared to Caco-2 cells, Tric-Caco2 cells showed significant 91% and 121% increases in resistance at 3 h and 4 h p.i., respectively (Fig. 7E). Moreover, the amount of FITC-dextran that crossed the Tric-Caco2 cell monolayers at 2 h, 3 h, and 4 h p.i. was significantly lower than that observed with Caco-2 cells (Fig. 7F). In addition, immunoblotting demonstrated increased tricellulin expression in Tric-Caco-2 cells compared to Caco-2 cells (Fig. 7G). However, it is important to note that the increased resistance observed in EPEC-infected Tric-Caco-2 cells was in part due to the high baseline resistance set by these cells before infection (Fig. 7E to G). Taken together, these results suggest that overexpression of tricellulin leads to increased resistance under both baseline and infection conditions, although it does not prevent EPEC from reducing TEER in Tric-Caco-2 cells compared to the peak TEER attained in uninfected cells.

DISCUSSION

TJs play a crucial role in the maintenance of intestinal epithelial barrier integrity, and their disruption by enteric pathogens and by inflammatory mediators in patients with IBD is one of the key mechanisms contributing to the pathophysiology of these diseases. Under physiological conditions, the intestinal epithelial barrier relies on

FIG 6 Maintenance of tricellulin expression is dependent on cytoskeletal microtubules. (A) Caco-2 cells infected with the Δ*espG1* mutant-FL, Δ*espG1* mutant-FL-ΔTB, Δ*espG1* Δ*espG2* mutant-FL, or Δ*espG1* Δ*espG2* mutant-FL-ΔTB strain were immunostained for β-tubulin (green) and nuclei (blue) and imaged by confocal microscopy. (B to E) Infected cells were measured for TEER (B and D) and FITC-dextran tracer fluorescence (C and E). The FITC fluorescence and TEER data are mean ± SEM values obtained from 3 independent experiments with 3 wells per condition. (F) Cell lysates obtained from the Δ*espG1* mutant-FL-ΔTB and Δ*espG1* Δ*espG2* mutant-FL-ΔTB strains were probed for tricellulin expression. (G) Immunolabeling of tricellulin (red) and nuclei (blue) on cells infected with the Δ*espG1* mutant-FL and Δ*espG1* Δ*espG2* mutant-FL strains for 4 h. Magnifications, ×2,000. (H) Caco-2 cells untreated or pretreated with nocodazole (10 μg/ml) for 1 h were infected with the WT EPEC and Δ*escN* strains. At 4 h p.i., cell lysates were probed for tricellulin expression by immunoblotting. For bar graph analysis of the Western blots, 3 independent experiments with 2 wells per condition were used. *, $P < 0.01$; **, $P < 0.001$; ***, $P < 0.0001$.

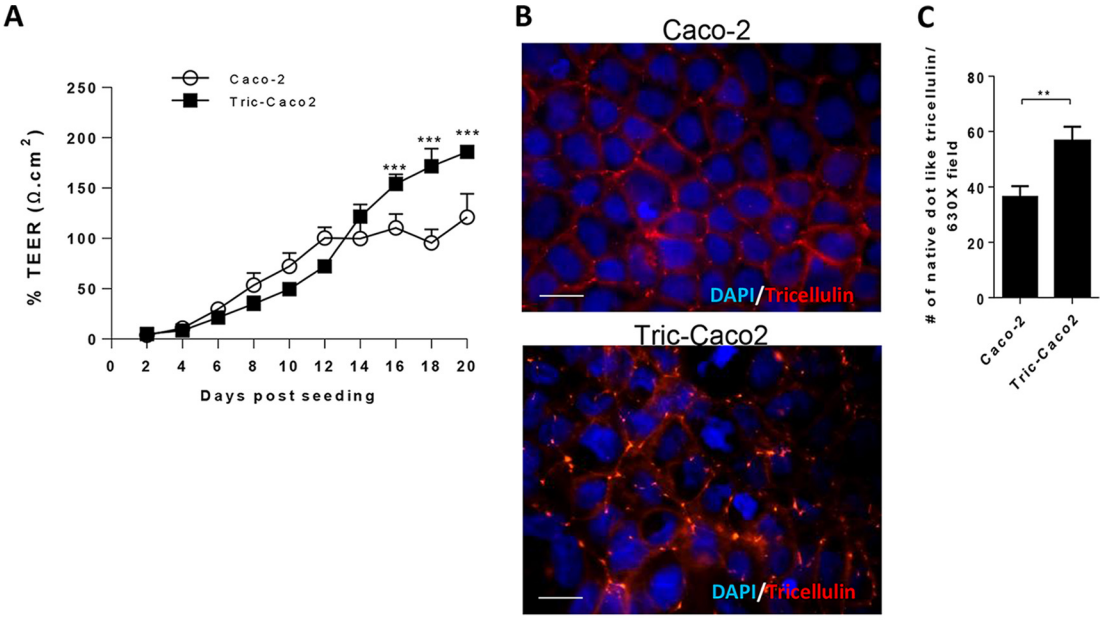
A
Caco-2
Tric-Caco2
% TEER (Ω.cm²)
Days post seeding
B
Caco-2
DAPI/Tricellulin
Tric-Caco2
DAPI/Tricellulin
C
# of native dot like tricellulin/ 630X field
Caco-2
Tric-Caco2

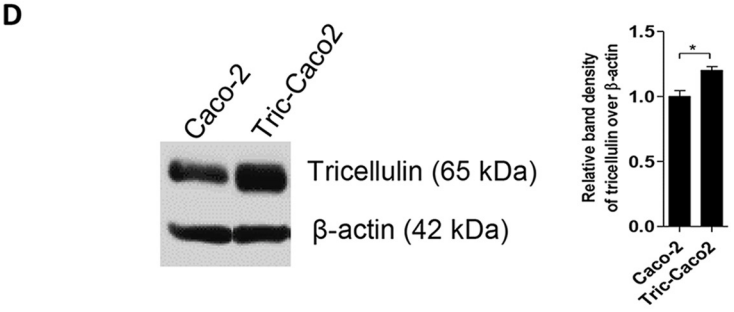
D
Caco-2
Tric-Caco2
Tricellulin (65 kDa)
β-actin (42 kDa)
Relative band density of tricellulin over β-actin
Caco-2
Tric-Caco2

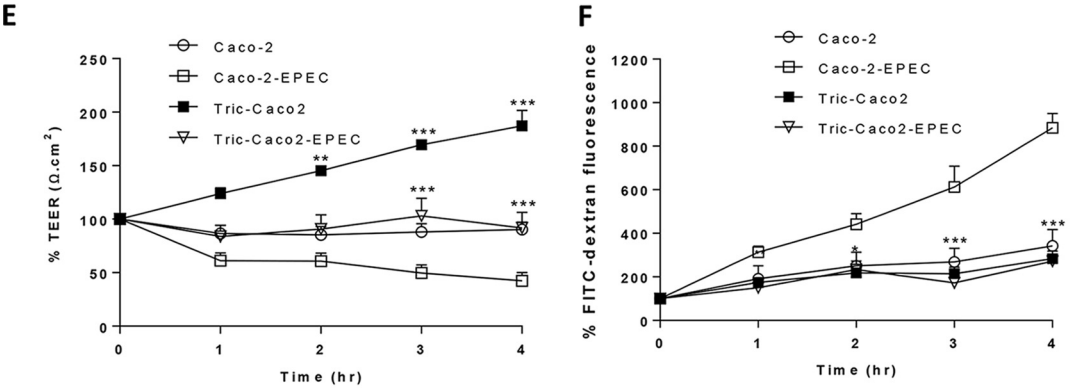
E
Caco-2
Caco-2-EPEC
Tric-Caco2
Tric-Caco2-EPEC
% TEER (Ω.cm²)
Time (hr)
F
Caco-2
Caco-2-EPEC
Tric-Caco2
Tric-Caco2-EPEC
% FITC-dextran fluorescence
Time (hr)


G
NI
EPEC
NI
EPEC
Tricellulin (65 kDa)
β-actin (42 kDa)
Caco-2
Tric-Caco2
CACO-2
TRIC-CACO2
Relative band density of tricellulin over β-actin
NI
EPEC
NI
EPEC

continuous strands of bi- and tricellular TJ proteins that form a tight seal between cells to prevent invasion by microbes and other extrinsic luminal antigens. However, enteric pathogenic bacteria, such as EPEC, *Salmonella*, and *Shigella*, have evolved key pathogenic strategies to disrupt this tight barrier, resulting in the loss of epithelial integrity (35–37). Several *in vivo* and *in vitro* studies have demonstrated a strong association between EPEC infection and the loss of TJ integrity (38–41). Of note, bTJ proteins, such as occludin, were shown to be dephosphorylated, resulting in their diffusion from the plasma membrane into the cytosol of epithelial cells during EPEC infection (41). In addition, it has also been observed that other bTJ proteins, such as claudin-1 and ZO-1, lose their apical localization, concurrent with the loss of barrier function during EPEC pathogenesis (12). Herein, we report for the first time that EPEC reduces tricellulin expression through EspG1-mediated microtubule disruption, resulting in the loss of epithelial resistance and barrier function.

The current study highlights the importance of the tTJ protein tricellulin in the maintenance of epithelial barrier integrity. Our results confirm that EPEC-induced epithelial barrier disruption is not restricted to bTJ proteins but can be extended to tTJs. Similar to previous observations in MDCK cells, we have also shown that overexpression of tricellulin in Caco-2 cells leads to the enhancement of barrier integrity with an increased TEER and a decreased paracellular permeability to 4-kDa macromolecules, although the effect seems to be partly dependent on the increased baseline resistance values set by Tric-Caco2 cells (22). Conversely and consistent with the findings of other studies, we show that the depletion of tricellulin in intestinal epithelial cells is associated with a loss of barrier integrity, characterized by a significant reduction in TEER and increased barrier permeability to macromolecules (19). Interestingly, the invasive enteropathogen *Shigella* has previously been shown to utilize tricellulin as part of its pathogenic strategy (23); however, unlike the disruptive effect of EPEC on tricellulin, *Shigella* was shown to exploit tricellulin to spread between adjoining cells (23). Contrary to the findings for *Shigella*, we speculate that EPEC-induced tricellulin disruption leads to increased intestinal epithelial permeability in order to provide nutrients from host cells.

Multiple type III secreted proteins, such as EspF, Map, and EspG1, have been associated with the disruption of TJ proteins; however, the precise mechanisms by which these effectors mediate their disruptive effects on the epithelial barrier function have not been fully defined (18, 30, 33, 42). Moreover, these effector proteins were shown to interfere with the distribution and function of bTJ proteins, while their role in modulating tTJs has not been explored to date. Studies on the EspF effector protein suggested that it can induce a dose-dependent reduction in TEER associated with occludin redistribution; however, infections with higher doses of the Δ*espF* EPEC mutant demonstrated a loss of TEER similar to that in WT EPEC, suggesting that EspF is not the only critical effector protein involved in the loss of barrier function (42). The effector protein Map, in association with the bacterial cell surface protein intimin, has also been implicated in the disruption of TJ integrity (18). By using Δ*espF*, Δ*map*, Δ*espG1*, and Δ*espG1* Δ*espG2* strains, we confirmed that both EspF and EspG1 are important for maintenance of epithelial barrier integrity. While a previous study has shown that the ectopic expression of EspG1 in MDCK epithelial cells leads to a selective paracellular permeability to 4-kDa dextran but not to high-molecular-mass (500-kDa) dextran (31), it did not reveal that EspG1 targeted TJ proteins that can modulate the

FIG 7 Tricellulin overexpression protects from the EPEC-induced loss of barrier integrity. (A) TEER measured in Tric-Caco2 cells and control Caco-2 cells. (B) Caco-2 and Tric-Caco2 cells grown for 21 days were immunostained for tricellulin (red) and nuclei (blue). Magnifications, ×1,000. (C) Quantitative analysis of the total number of tricellulin-positive dot-like structures present at tTJs. A total of 10 images were analyzed at magnifications of ×630 for quantification. (D) Cell lysates obtained from Tric-Caco2 and control Caco-2 cells were probed for tricellulin expression. (E and F) Tric-Caco2 and control Caco-2 cells were infected with WT EPEC and measured for TEER (E) and FITC-dextran tracer fluorescence. (F). (G) Tric-Caco2 and control Caco-2 cells infected with WT EPEC were probed for tricellulin expression. The TEER and FITC fluorescence data presented in panels A, E, and F are mean ± SEM values obtained from 4 independent experiments with 3 wells per condition. A minimum of 3 independent experiments with 2 to 3 wells per condition were used for analysis. *, $P < 0.01$; **, $P < 0.001$; ***, $P < 0.0001$.

epithelial barrier function. Our results revealed that tricellulin expression levels were significantly reduced in cells infected with the WT EPEC, Δ*espG1* mutant-FL, or Δ*espG1* Δ*espG2* mutant-FL strain (in which the last two strains were complemented with full-length EspG1) but not in cells infected with noncomplemented Δ*espG1* and Δ*espG1* Δ*espG2* strains, suggesting a role for EspG1 in reducing tricellulin expression. Indeed, our results show that EspG1 but not EspF is required to alter the expression of tricellulin (Fig. 3C). Whether EspG2, a homologue of EspG1, plays a similar role in altering tricellulin expression will be determined in future studies.

Several studies have implicated microtubule disruption as one of the mechanisms by which EspG1 contributes to EPEC-induced disruption of the epithelial barrier function (13, 17, 33). In addition to supporting a similar mechanism, our study also shows that a putative tubulin binding domain of EspG1 plays a key role in mediating EspG1-induced microtubule disruption. While it is possible that this domain interacts with tubulin (directly or indirectly), it may also help to maintain the proper structure of EspG1. Recently, EspG1 was shown to harbor Tre-2/Bub2/Cdc16 (TBC)-like two-catalytic-finger motifs (glutamine and arginine) for Rab 1 and enzymatic motifs for ADP-ribosylation factor (ARF) GTPases and p21-activated kinases (PAKs) (43–45). Interestingly, the glutamine finger motif (YXQ) and PAK binding motif (N212/N323) overlap the putative tubulin binding domain. While the above-described enzymatic motifs are important for EspG1-induced disruption in endoplasmic reticulum-to-Golgi apparatus trafficking, their roles in EspG1-induced microtubule disruption still remain to be explored.

Using a genetic approach, we have shown that infection with the Δ*espG1* mutant maintained tricellulin expression levels similar to those in uninfected cells, suggesting a strong correlation between the functioning/presence of microtubules and the normal expression of tricellulin. Moreover, the observation that infections with the Δ*espG1* mutant-FL-ΔTB and Δ*espG1* Δ*espG2* mutant-FL-ΔTB strains resulted in a minimal effect on tricellulin expression further supports our hypothesis that microtubule stability impacts the expression of tricellulin. However, at this stage, it is unclear whether tricellulin modulation by EPEC is a direct effect of microtubule disruption or is indirectly mediated via the loss of function of other bTJ proteins (such as occludin), as demonstrated by Glotfelty et al. (17). Although phylogenetic analysis of occludin, tricellulin, and MARVELD3 (MAL and related proteins for vesicle trafficking and membrane linkD3) revealed a common conserved four-transmembrane MARVEL domain in their protein structures, these proteins were shown to be functionally independent of each other in regulating TJ function (20). Future mechanistic studies using cell lines that lack occludin and tricellulin could provide a better understanding of their roles in EPEC pathogenesis.

In summary, we have shown that during EPEC infection, expression of the tTJ protein tricellulin is severely disrupted by the T3SS effector EspG1, resulting in reduced barrier resistance and increased permeability. Furthermore, our results show that tricellulin overexpression positively modulated the epithelial barrier function during EPEC infection. Since tricellulin is a key protein in maintaining the integrity of the epithelial barrier, enhancing its expression may offer beneficial effects in intestinal diseases associated with EPEC infections. However, it is important to consider potential adverse effects that may occur due to reduced barrier permeability and increased stability. Consequently, future studies using *in vivo* models will need to address the potential therapeutic benefits of tricellulin overexpression under intestinal inflammatory conditions.

MATERIALS AND METHODS

Cell cultures. Approximately 5×10^5 Caco-2 epithelial cells obtained from a 72-year-old male Caucasian (ATCC) were seeded either in 0.33-cm^2 permeable polyester Transwell filters with a 0.4-μm pore size (Costar; Corning) or in 12- or 6-well tissue culture plates. Cells were grown in complete medium containing high-glucose Dulbecco modified Eagle medium (DMEM; Gibco) with 10% fetal bovine serum (FBS), 1× minimum essential medium (MEM), 15 mM HEPES, and 50 U/ml penicillin-streptomycin. A humid incubator that was set at 37°C and in which CO_2 levels were maintained at 5% was used to culture

TABLE 1 Bacterial strains and plasmids used in the study

Bacterial strain or genotype or plasmid	Description	Source or reference
Strains		
AIEC	Serotype O83:H1	48
WT EPEC 2348/69	O127:H6 isolate	49
Δ*escN*	Deletion of *escN* from WT EPEC	49
Δ*espF*	Deletion of *espF* from WT EPEC	50
Δ*map*	Deletion of *map* from WT EPEC	51
Δ*espH*	Deletion of *espH* from WT EPEC	30
Δ*espG1*	Deletion of *espG1* from WT EPEC	This study
Δ*espG1* Δ*espG2*	Deletion of *espG2* from Δ*espG1* strain	This study
Δ*espG1*-FL	Δ*espG1* mutant complemented with full-length *espG1*	This study
Δ*espG1* Δ*espG2*-FL	Δ*espG1* Δ*espG2* mutant complemented with full-length *espG1*	This study
Δ*espG1*-FL-ΔTB	Δ*espG1* mutant complemented with *espG1* that lacks a putative tubulin binding domain	This study
Δ*espG1* Δ*espG2*-FL-ΔTB	Δ*espG1* Δ*espG2* mutant complemented with *espG1* that lacks a putative tubulin binding domain	This study
WT EPEC (GFP)	WT EPEC transformed with GFP-expressing plasmid pFPV25.1	This study
Δ*escN* (GFP)	Δ*escN* mutant transformed with GFP-expressing plasmid pFPV25.1	This study
Δ*espG1* (GFP)	Δ*espG1* mutant transformed with GFP-expressing plasmid pFPV25.1	This study
Δ*espG1* Δ*espG2* (GFP)	Δ*espG1* Δ*espG2* mutant transformed with GFP-expressing plasmid pFPV25.1	This study
Plasmids		
pFPV25.1	GFPmut3a is expressed constitutively, ampicillin resistant	52
pTOPO-2HA	pCR2.1-TOPO-based expression vector, ampicillin and kanamycin resistant	53
pEspG1-FL	pTOPO-*espG1*-FL, ampicillin and kanamycin resistant	This study
pEspG1-ΔTB	pTOPO-*espG1*-FL-ΔTB, ampicillin and kanamycin resistant	This study
pRE112	Suicide vector, chloramphenicol resistant	47
pRE112-Δ*espG2*	pRE112-based construct used to make the Δ*espG2* deletion mutant	This study

the cells. For cells grown on Transwells, 500 μl of complete medium was used in the upper chamber, where the cells were seeded, and 1.5 ml was used in the bottom chamber. Cells were grown for a period of 19 to 21 days, with the medium being changed every 2 days. Prior to EPEC infection, the medium was switched to high-glucose DMEM containing 2% FBS with no MEM, HEPES, or antibiotics.

Generation of Tric-Caco2 cells. To generate a stable Caco-2 cell line that overexpresses tricellulin (Tric-Caco2), we made a plasmid construct consisting of a pBluescript backbone, tricellulin expressed under the control of a cytomegalovirus (CMV) promoter, and a puromycin resistance selection cassette by a three-way ligation method. Briefly, a pCMV-Sport6-tricellulin vector was digested with NsiI and ClaI, resulting in the release of a CMV promoter-tricellulin-containing fragment. The fragment containing the puromycin resistance selection cassette was obtained by digesting the pPGK-puromycin-containing vector with ClaI/XhoI. Similarly, the fragment containing the pBluescript backbone was obtained by digesting the pBluescript vector with restriction enzymes PstI (PstI and NsiI have comparable 3′ overhangs) and XhoI. These three fragments were then ligated in the presence of T4 ligase, followed by transformation into *E. coli* DH10B. DNA sequencing was used to confirm that the plasmids contained the correct inserts, and then the plasmids were transfected into Caco-2 cells using the Fugene HD transfection reagent (Roche). Transfected cells were selected in the presence of puromycin (2 μg/ml) for 10 days and enriched to produce a population of Caco-2 cells overexpressing tricellulin.

Bacterial strains and growth conditions. Caco-2 cells grown until days 19 to 21 were infected with either adherent-invasive *E. coli* (AIEC) or EPEC. WT EPEC and mutant strains that lack genes encoding type III secretion system structural factors or effectors, such as the Δ*escN*, Δ*espF*, Δ*map*, Δ*espH*, Δ*espG1*, and Δ*espG1* Δ*espG2* mutant strains and the Δ*espG1* and Δ*espG1* Δ*espG2* mutant strains complemented with either full-length *espG1* or full-length *espG1* and *espG2* that lacks a putative tubulin binding domain, were used for all infections (Table 1). All bacteria were grown overnight in LB broth, and their optical density at 600 nm was measured to evaluate the number of bacteria per milliliter. After centrifugation at 3,000 rpm for 5 min, the bacterial pellet was washed in phosphate-buffered saline (PBS) 3 times and resuspended in 2% DMEM containing 1 mg/ml FITC conjugated to dextran (4 kDa). A multiplicity of infection (MOI) of 100:1 (bacterial cells to epithelial cells) was used for infection studies.

Transepithelial electrical resistance. TEER measurements were taken at 0, 1, 2, 3, and 4 h p.i. by using a voltmeter (World Precision Instruments) according to the manufacturer's recommendations. After subtraction of the TEER values measured with the bathing solution (~120 $\Omega \cdot cm^2$), the 0-h TEER readings were normalized to 100 $\Omega \cdot cm^2$ and considered 100%. On the basis of these initial readings, the percent change in values for the other time points were calculated.

Paracellular permeability. FITC-conjugated dextran (1 mg/ml) was added to the upper chamber of Transwells containing 2% DMEM. At 0, 1, 2, 3, and 4 h p.i., 100 μl of sample was collected from the lower chamber to quantify the amount of FITC-dextran that reached the chamber. The 100-μl sample was replaced at each time point by adding 100 μl of 2% FBS containing DMEM back into the lower chamber. Fluorescence was read using a Wallac Victor fluorimeter (PerkinElmer Life Sciences) that detects the fluorescence at excitation and emission wavelengths of 495 nm and 519 nm, respectively. The data

TABLE 2 Primer sets used in this study

Target mRNA	Orientation	Sequence
Tricellulin	Forward	5′-TCAGACAGATGATGAGCGAGA-3′
	Reverse	5′-ATGTTCCTGTCGGCTTTCC-3′
Occludin	Forward	5′-TCCAATGGCAAAGTGAATGA-3′
	Reverse	5′-AGTCCTCCTCCAGCTCATCA-3′
Claudin-1	Forward	5′-CGATGAGGTGCAGAAGATGA-3′
	Reverse	5′-ATGCTTGCTACCCTTGGACCAC-3′
18S rRNA	Forward	5′-CAGCCACCCCGAGATTGAGCA-3′
	Reverse	5′-TAGTAGCGACGGGCGGTGTG-3′

obtained at 0 h were normalized to 100 fluorescence units (FU) and are represented as 100%. The percent changes from the 1-h to the 4-h time points were calculated on the basis of these initial readings.

Immunocytochemistry. Caco-2 cells grown on glass coverslips placed in each well of a 24-well plate were used for immunofluorescence studies. Cells were infected for 4 h with an EPEC strain transformed with a GFP-expressing plasmid, at which point the medium was removed and the cells were fixed in 3.7% PFA for 15 min at 4°C. After permeabilization in 0.3% SDS for 5 min, the cells were blocked in biotin block A and B (Life Technologies) (45 min each) and 1% bovine serum albumin (BSA) with goat serum for 60 min, followed by overnight incubation with rabbit antitricellulin (Life Technologies) and goat GFP-biotin-labeled (GeneTex) primary antibodies (1:200). On the following day, the cells were washed in PBS and incubated for 1 h with anti-rabbit immunoglobulin secondary antibodies conjugated to Alexa Fluor 488 and 568 (1:2,000). The cells were finally mounted with ProLong Gold antifade reagent containing DAPI (4′,6-diamidino-2-phenylindole; Invitrogen). The slides were viewed under a confocal imaging system (Leica TCS SP5 system) that uses Leica Application suite software or a Zeiss AxioImager fluorescence microscope connected to an AxioCam HRm camera to capture images.

Gene expression analysis by qPCR. Total RNA was extracted from uninfected and infected Caco-2 cells using a Qiagen RNeasy kit following the manufacturer's protocol. The total amount of RNA extracted was quantified using a NanoDrop spectrophotometer (ND1000). One microgram of RNA was used to generate cDNA by using random primers obtained from a Qiagen Omniscript reverse transcription kit. To run a PCR, a total of 5 μl of cDNA (diluted in RNase- and DNase-free water at 1:5) was added to 15 μl of a PCR mix containing 10 μl SYBR green dye (Bio-Rad) and 5 μl comprised of RNase- and DNase-free water and primers to a final concentration of 0.6 μM. All reaction mixtures were assembled in duplicate, and quantitative PCR (qPCR) was carried out using a Bio-Rad Opticon2 system. Melting point analysis confirmed the specificity of the PCR. Results were quantified using GeneEx Macro OM (version 3.0) software (Bio-Rad) following the $2\Delta\Delta C_T$ threshold cycle (C_T) method. The primer sequences are given in Table 2. The reaction schemes were as follows: all PCRs had an initial denaturing step of 95°C for 3 to 5 min, followed by another step of denaturation at 94°C for 30 s, annealing at a temperature of 55°C for 30 s (tricellulin and occludin) or 60°C for 30 s (claudin-1 and 18S rRNA), and a final extension at 72°C for 30 s.

Knockdown of tricellulin expression by RNA interference. Knockdown of tricellulin expression was carried out by using small interfering RNA (siRNA). Briefly, tricellulin-specific siRNA (Thermo Fischer) and a negative-control siRNA (Thermo Fischer) were each combined with the RNAiMAX transfecting agent (Gibco) and diluted to a final concentration of 200 nM and 400 nM in Opti-MEM medium (Gibco). For transfection, approximately 3×10^5 Caco-2 cells were mixed with the siRNA mix described above and seeded on the upper chamber of a Transwell plate. Cells were grown until day 3 postseeding, at which time the medium was changed. TEER and FITC-dextran fluorescence readings were taken daily for a period of 6 days. A second round of transfection was performed on day 4 postseeding for the collection of lysates on day 8 to detect tricellulin protein expression by Western blotting.

Western blot analysis of Caco-2 cell lysates. Western blot analysis was performed on Caco-2 cells that had been grown for 19 to 21 days and either treated with nocodazole or siRNA or infected with WT or mutant EPEC strains. After 4 h of treatment or infection, cells were washed 3 times with sterile PBS, followed by lysis of the cells with radioimmunoprecipitation assay buffer (150 mM sodium chloride, 1% Triton X-100, 0.5% sodium deoxycholate, 0.1% sodium dodecyl sulfate [SDS], 50 mM Tris, pH 8.0, along with phosphatase inhibitor tablets [Roche] and a protease inhibitor cocktail for bacterial cell extracts [Sigma]). The lysates were then resolved by SDS-PAGE and transferred onto 0.2-μm polyvinylidene difluoride membranes (GE). Membranes were blocked with 5% BSA (Sigma) and probed using human antitricellulin or claudin-3 (both purchased from Thermo Fisher) or β-actin (Cell Signaling), all of which were used at a 1:2,000 dilution. The blots were incubated with horseradish peroxidase-conjugated anti-rabbit immunoglobulin secondary antibody (1:10,000 dilution; Cell Signaling) and exposed to SuperSignal West Dura substrate (Thermo Fisher), followed by visualization of the protein bands by a ChemiDoc XRS system (Bio-Rad). The band intensities were semiquantified by ImageJ software and were normalized against the intensities of β-actin bands. The results are presented as means $\pm$ standard errors of the means (SEMs).

Generation of Δ*espG1* and Δ*espG1* Δ*espG2* mutants. To generate the Δ*espG1* mutant, a previously used suicide vector (pCVD442) containing an in-frame deletion of *espG1* (44) was transformed into SM10λ *pir*, and the resulting strain was conjugated with wild-type EPEC strain E2348/69 (streptomycin resistant) for 24 h at 37°C. The conjugated colonies were selected on LB agar plates containing ampicillin (100 μg/ml) and streptomycin (100 μg/ml) to generate single-crossover mutants. To obtain the double-

crossover (i.e., deletion) mutants, single-crossover mutants were cultured in LB (no salt) for 8 h at 37°C before being plated onto LB agar plates containing 5% sucrose and cultured at 37°C for another 24 h. The mutant colonies were screened by PCR.

Overlap extension PCR (46) was used to generate the in-frame deletion of *espG2* for the Δ*espG1* mutant. To generate the Δ*espG2* construct, two PCR fragments were amplified using EPEC E2348/69 genomic DNA as the template. The primer pairs used to amplify the PCR fragments were *espG2*-P1 (5′-GCACG*TCTAGA*GGACATTGTTAAACTCATCGGACGGGTA-3′) plus *espG2*-P2 (5′-CTGAGCTGAATTTGACTG AATAGACCTCAGT-3′) and *espG2*-P3 (5′-GTCAAATTCAGCTCAGGAGCTCGTTCGAGTGATTAAACCCAT TTA-3′) plus *espG2*-P4 (5′-GCACG*TCTAGA*GTTGCTGTGACACTATAAGCTCCACCTA-3′), respectively. This results in a 951-bp fragment containing the upstream sequence of *espG2* and a 997-bp fragment containing the downstream sequence of *espG2*, respectively. These two PCR fragments were then mixed and used as the template for a secondary PCR (with primer pair *espG2*-P1 and *espG2*-P4, both of which contain an XbaI restriction enzyme site [shown in italics]). The 16-bp overlapping sequence (underlined) in primers *espG2*-P2 and *espG2*-P3 allows the amplification of a 1,848-bp PCR product. The PCR product was digested with XbaI and directly cloned into a suicide vector, pRE112 (Cm^r) (47). DNA sequencing was performed to confirm that the Δ*espG2* construct was correct. This pRE112-based Δ*espG2* mutant construct was then transformed into SM10λ *pir*, and the resulting strain was conjugated with the Δ*espG1* mutant for 24 at 37°C. The conjugated colonies were selected on LB agar plates containing chloramphenicol (30 μg/ml) and streptomycin (100 μg/ml) to generate single-crossover mutants (34). The Δ*espG1* Δ*espG2* mutants were then obtained as described above for the Δ*espG1* mutant.

Generation of strains complemented with full-length *espG1* (*espG1* mutant-FL) or partial *espG1* lacking a putative tubulin binding domain (*espG1* mutant-FL-ΔTB). PCR fragments containing the *espG1*-FL or *espG1*-FL-ΔTB sequence were amplified using EPEC E2348/69 genomic DNA as the template. The *espG1*-FL fragment, containing the promoter region of *espG1* and the entire coding sequence of *espG1* (except for the stop codon), was amplified using primer pairs *espG1*-P1 and *espG1*-P4. The *espG1*-FL-ΔTB fragment was obtained using an overlap extension PCR as described above. Briefly, the primer pairs *espG1*-P1 (5′-GACTT*GAGCTC*CTGTTCTTTGTCGCACCTATCGATCG-3′) plus *espG1*-P2 (5′-ACCA TTGAGTGAAAGCTTTGCATTGCCGA-3′) and *espG1*-P3 (5′-GCTTTCACTCAATGGTTCATCAGATGGAAACA-3′) plus *espG1*-P4 (5′-GCTCT*CTCGAG*AGTGTTTTGTAAGTACGTTTCAGATGCG-3′) were used to amplify a 1,223-bp fragment containing the upstream sequence of *espG1* and a 198-bp fragment containing the downstream sequence of *espG1*, respectively. Restriction enzyme sites (SacI and XhoI) in the primer sequences are italicized, whereas the overlapping sequences in the primers are underlined. The two PCR fragments containing the upstream and downstream sequences of *espG1* were then mixed and used as the template for a secondary PCR (with primer pairs *espG1*-P1 and *espG1*-P4), resulting in the deletion of the putative tubulin binding domain of *espG1* (i.e., the *espG1*-FL-ΔTB fragment lacking amino acids 220 to 332). The *espG1*-FL and *espG1*-FL-ΔTB fragments were then digested with SacI and XhoI restriction enzymes and cloned into plasmid pTOPO-2HA (34) by using *E. coli* strain DH10B, resulting in pTOPO-*espG1*-FL and pTOPO-*espG1*-FL-ΔTB, respectively. The identity of pTOPO-*espG1*-FL and pTOPO-*espG1*-FL-ΔTB was verified by DNA sequencing before transformation into the Δ*espG1* or Δ*espG1* Δ*espG2* mutant by electroporation.

Statistical analysis. Statistical analysis was carried out using GraphPad Prism software (version 6; GraphPad Software, San Diego, CA, USA). Significance was calculated using an unpaired Student's *t* test. Single and multiple analyses of variance followed by the Bonferroni or Tukey *post hoc* test were used as appropriate.

ACKNOWLEDGMENTS

This work was supported by a grant from the Crohn's and Colitis Foundation of Canada (CCC) to K.J. V.M. holds a joint Michael Smith Foundation for Health Research/ CCFC postdoctoral fellowship. F.A.G. holds a salary award from the Experimental Medicine Program, University of British Columbia. M.S. holds a salary award from the Michael Smith Foundation for Health Research. B.A.V. is the Children with Intestinal and Liver Disorders (CHILD) Foundation Chair in Pediatric Gastroenterology and the Canada Research Chair in Pediatric Gastroenterology. K.J. is a senior clinician scientist supported by the British Columbia Children's Hospital Research Institute Clinician Scientists Award Program, University of British Columbia, and is also supported by the CHILD Foundation.

V.M., V.S.C., B.A.V., H.B.Y., and K.J. conceived of and designed the experiments. V.M., F.A.G., M.S., U.D., V.S.C., T.H., and H.B.Y. performed the experiments. V.M., F.A.G., M.S., U.D., B.A.V., H.B.Y., and K.J. analyzed the data. V.M., F.A.G., M.S., U.D., V.S.C., T.H., and H.B.Y. contributed reagents, materials, or analysis tools. V.W., F.A.G., and M.S. prepared the figures. V.M., B.A.V., H.B.Y., and K.J. wrote the paper. All authors reviewed the manuscript.

We declare no competing financial interests.

REFERENCES

1. Kunyoo S, Vanessa CF, Ben M. 2006. Tight junctions and cell polarity. Cell Dev Biol 22:207–235. https://doi.org/10.1146/annurev.cellbio.22.010305.104219.
2. Aijaz S, Balda MS, Matter K. 2006. Tight junctions: molecular architecture and function. Int Rev Cytol 248:261–298. https://doi.org/10.1016/S0074-7696(06)48005-0.
3. Steed E, Balda MS, Matter K. 2010. Dynamics and functions of tight junctions. Trends Cell Biol 20:142–149. https://doi.org/10.1016/j.tcb.2009.12.002.
4. Niessen CM. 2007. Tight junctions/adherens junctions: basic structure and function. J Invest Dermatol 127:2525–2532. https://doi.org/10.1038/sj.jid.5700865.
5. Tang VW, Goodenough DA. 2003. Paracellular ion channel at the tight junction. Biophys J 84:1660–1673. https://doi.org/10.1016/S0006-3495(03)74975-3.
6. Nusrat A, Turner JR, Madara JL. 2000. Molecular physiology and pathophysiology of tight junctions. IV. Regulation of tight junctions by extracellular stimuli: nutrients, cytokines, and immune cells. Am J Physiol Gastrointest Liver Physiol 279:G851–G857.
7. Dean P, Maresca M, Schuller S, Phillips AD, Kenny B. 2006. Potent diarrheagenic mechanism mediated by the cooperative action of three enteropathogenic *Escherichia coli*-injected effector proteins. Proc Natl Acad Sci U S A 103:1876–1881. https://doi.org/10.1073/pnas.0509451103.
8. Hecht G, Hodges K, Gill RK, Kear F, Tyagi S, Malakooti J, Ramaswamy K, Dudeja PK. 2004. Differential regulation of Na^+/H^+ exchange isoform activities by enteropathogenic *E. coli* in human intestinal epithelial cells. Am J Physiol Gastrointest Liver Physiol 287:G370–G378. https://doi.org/10.1152/ajpgi.00432.2003.
9. Glotfelty LG, Hecht GA. 2012. Enteropathogenic *E. coli* effectors EspG1/G2 disrupt tight junctions: new roles and mechanisms. Ann N Y Acad Sci 1258:149–158. https://doi.org/10.1111/j.1749-6632.2012.06563.x.
10. Dean P, Kenny B. 2009. The effector repertoire of enteropathogenic *E. coli*: ganging up on the host cell. Curr Opin Microbiol 12:101–109. https://doi.org/10.1016/j.mib.2008.11.006.
11. Vallance BA, Finlay BB. 2000. Exploitation of host cells by enteropathogenic *Escherichia coli*. Proc Natl Acad Sci U S A 97:8799–8806. https://doi.org/10.1073/pnas.97.16.8799.
12. Muza-Moons MM, Schneeberger EE, Hecht GA. 2004. Enteropathogenic *Escherichia coli* infection leads to appearance of aberrant tight junctions strands in the lateral membrane of intestinal epithelial cells. Cell Microbiol 6:783–793. https://doi.org/10.1111/j.1462-5822.2004.00404.x.
13. Shaw RK, Smollett K, Cleary J, Garmendia J, Straatman-Iwanowska A, Frankel G, Knutton S. 2005. Enteropathogenic *Escherichia coli* type III effectors EspG and EspG2 disrupt the microtubule network of intestinal epithelial cells. Infect Immun 73:4385–4390. https://doi.org/10.1128/IAI.73.7.4385-4390.2005.
14. Abe A, de Grado M, Pfuetzner RA, Sanchez-Sanmartin C, Devinney R, Puente JL, Strynadka NC, Finlay BB. 1999. Enteropathogenic *Escherichia coli* translocated intimin receptor, Tir, requires a specific chaperone for stable secretion. Mol Microbiol 33:1162–1175.
15. Rodriguez-Escudero I, Hardwidge PR, Nombela C, Cid VJ, Finlay BB, Molina M. 2005. Enteropathogenic *Escherichia coli* type III effectors alter cytoskeletal function and signalling in Saccharomyces cerevisiae. Microbiology 151:2933–2945. https://doi.org/10.1099/mic.0.28072-0.
16. Weflen AW, Alto NM, Hecht GA. 2009. Tight junctions and enteropathogenic E coli. Ann N Y Acad Sci 1165:169–174. https://doi.org/10.1111/j.1749-6632.2009.04060.x.
17. Glotfelty LG, Zahs A, Hodges K, Shan K, Alto NM, Hecht GA. 2014. Enteropathogenic *E. coli* effectors EspG1/G2 disrupt microtubules, contribute to tight junction perturbation and inhibit restoration. Cell Microbiol 16:1767–1783. https://doi.org/10.1111/cmi.12323.
18. Dean P, Kenny B. 2004. Intestinal barrier dysfunction by enteropathogenic *Escherichia coli* is mediated by two effector molecules and a bacterial surface protein. Mol Microbiol 54:665–675. https://doi.org/10.1111/j.1365-2958.2004.04308.x.
19. Ikenouchi J, Furuse M, Furuse K, Sasaki H, Tsukita S, Tsukita S. 2005. Tricellulin constitutes a novel barrier at tricellular contacts of epithelial cells. J Cell Biol 171:939–945. https://doi.org/10.1083/jcb.200510043.
20. Raleigh DR, Marchiando AM, Zhang Y, Shen L, Sasaki H, Wang Y, Long M, Turner JR. 2010. Tight junction-associated MARVEL proteins marveld3, tricellulin, and occludin have distinct but overlapping functions. Mol Biol Cell 21:1200–1213. https://doi.org/10.1091/mbc.E09-08-0734.
21. Riazuddin S, Ahmed ZM, Fanning AS, Lagziel A, Kitajiri S, Ramzan K, Khan SN, Chattaraj P, Friedman PL, Anderson JM, Belyantseva IA, Forge A, Riazuddin S, Friedman TB. 2006. Tricellulin is a tight-junction protein necessary for hearing. Am J Hum Genet 79:1040–1051. https://doi.org/10.1086/510022.
22. Krug SM, Amasheh S, Richter JF, Milatz S, Gunzel D, Westphal JK, Huber O, Schulzke JD, Fromm M. 2009. Tricellulin forms a barrier to macromolecules in tricellular tight junctions without affecting ion permeability. Mol Biol Cell 20:3713–3724. https://doi.org/10.1091/mbc.E09-01-0080.
23. Fukumatsu M, Ogawa M, Arakawa S, Suzuki M, Nakayama K, Shimizu S, Kim M, Mimuro H, Sasakawa C. 2012. *Shigella* targets epithelial tricellular junctions and uses a noncanonical clathrin-dependent endocytic pathway to spread between cells. Cell Host Microbe 11:325–336. https://doi.org/10.1016/j.chom.2012.03.001.
24. Morampudi V, Conlin VS, Dalwadi U, Wu X, Marshall KC, Nguyen C, Vallance BA, Jacobson K. 2015. Vasoactive intestinal peptide prevents PKCε-induced intestinal epithelial barrier disruption during EPEC infection. Am J Physiol Gastrointest Liver Physiol 308:G389–G402. https://doi.org/10.1152/ajpgi.00336.2014.
25. Conlin VS, Wu X, Nguyen C, Dai C, Vallance BA, Buchan AM, Boyer L, Jacobson K. 2009. Vasoactive intestinal peptide ameliorates intestinal barrier disruption associated with *Citrobacter rodentium*-induced colitis. Am J Physiol Gastrointest Liver Physiol 297:G735–G750. https://doi.org/10.1152/ajpgi.90551.2008.
26. Li Q, Zhang Q, Wang C, Li N, Li J. 2008. Invasion of enteropathogenic *Escherichia coli* into host cells through epithelial tight junctions. FEBS J 275:6022–6032. https://doi.org/10.1111/j.1742-4658.2008.06731.x.
27. Masuda S, Oda Y, Sasaki H, Ikenouchi J, Higashi T, Akashi M, Nishi E, Furuse M. 2011. LSR defines cell corners for tricellular tight junction formation in epithelial cells. J Cell Sci 124:548–555. https://doi.org/10.1242/jcs.072058.
28. Ikenouchi J, Sasaki H, Tsukita S, Furuse M, Tsukita S. 2008. Loss of occludin affects tricellular localization of tricellulin. Mol Biol Cell 19:4687–4693. https://doi.org/10.1091/mbc.E08-05-0530.
29. Viswanathan VK, Koutsouris A, Lukic S, Pilkinton M, Simonovic I, Simonovic M, Hecht G. 2004. Comparative analysis of EspF from enteropathogenic and enterohemorrhagic *Escherichia coli* in alteration of epithelial barrier function. Infect Immun 72:3218–3227. https://doi.org/10.1128/IAI.72.6.3218-3227.2004.
30. Tu X, Nisan I, Yona C, Hanski E, Rosenshine I. 2003. EspH, a new cytoskeleton-modulating effector of enterohaemorrhagic and enteropathogenic *Escherichia coli*. Mol Microbiol 47:595–606. https://doi.org/10.1046/j.1365-2958.2003.03329.x.
31. Matsuzawa T, Kuwae A, Abe A. 2005. Enteropathogenic *Escherichia coli* type III effectors EspG and EspG2 alter epithelial paracellular permeability. Infect Immun 73:6283–6289. https://doi.org/10.1128/IAI.73.10.6283-6289.2005.
32. Elliott SJ, Krejany EO, Mellies JL, Robins-Browne RM, Sasakawa C, Kaper JB. 2001. EspG, a novel type III system-secreted protein from enteropathogenic *Escherichia coli* with similarities to VirA of *Shigella flexneri*. Infect Immun 69:4027–4033. https://doi.org/10.1128/IAI.69.6.4027-4033.2001.
33. Tomson FL, Viswanathan VK, Kanack KJ, Kanteti RP, Straub KV, Menet M, Kaper JB, Hecht G. 2005. Enteropathogenic *Escherichia coli* EspG disrupts microtubules and in conjunction with Orf3 enhances perturbation of the tight junction barrier. Mol Microbiol 56:447–464. https://doi.org/10.1111/j.1365-2958.2005.04571.x.
34. Hardwidge PR, Deng W, Vallance BA, Rodriguez-Escudero I, Cid VJ, Molina M, Finlay BB. 2005. Modulation of host cytoskeleton function by the enteropathogenic *Escherichia coli* and *Citrobacter rodentium* effector protein EspG. Infect Immun 73:2586–2594. https://doi.org/10.1128/IAI.73.5.2586-2594.2005.
35. Ibarra JA, Steele-Mortimer O. 2009. *Salmonella*—the ultimate insider. Salmonella virulence factors that modulate intracellular survival. Cell Microbiol 11:1579–1586. https://doi.org/10.1111/j.1462-5822.2009.01368.x.
36. Schroeder GN, Hilbi H. 2008. Molecular pathogenesis of *Shigella* spp.: controlling host cell signaling, invasion, and death by type III secretion. Clin Microbiol Rev 21:134–156. https://doi.org/10.1128/CMR.00032-07.
37. Coburn B, Sekirov I, Finlay BB. 2007. Type III secretion systems and

disease. Clin Microbiol Rev 20:535–549. https://doi.org/10.1128/CMR.00013-07.
38. Spitz J, Yuhan R, Koutsouris A, Blatt C, Alverdy J, Hecht G. 1995. Enteropathogenic *Escherichia coli* adherence to intestinal epithelial monolayers diminishes barrier function. Am J Physiol 268:G374–G379.
39. Shifflett DE, Clayburgh DR, Koutsouris A, Turner JR, Hecht GA. 2005. Enteropathogenic *E. coli* disrupts tight junction barrier function and structure in vivo. Lab Invest 85:1308–1324. https://doi.org/10.1038/labinvest.3700330.
40. Canil C, Rosenshine I, Ruschkowski S, Donnenberg MS, Kaper JB, Finlay BB. 1993. Enteropathogenic *Escherichia coli* decreases the transepithelial electrical resistance of polarized epithelial monolayers. Infect Immun 61:2755–2762.
41. Simonovic I, Rosenberg J, Koutsouris A, Hecht G. 2000. Enteropathogenic *Escherichia coli* dephosphorylates and dissociates occludin from intestinal epithelial tight junctions. Cell Microbiol 2:305–315. https://doi.org/10.1046/j.1462-5822.2000.00055.x.
42. McNamara BP, Koutsouris A, O'Connell CB, Nougayrede JP, Donnenberg MS, Hecht G. 2001. Translocated EspF protein from enteropathogenic *Escherichia coli* disrupts host intestinal barrier function. J Clin Invest 107:621–629. https://doi.org/10.1172/JCI11138.
43. Dong N, Zhu Y, Lu Q, Hu L, Zheng Y, Shao F. 2012. Structurally distinct bacterial TBC-like GAPs link Arf GTPase to Rab1 inactivation to counteract host defenses. Cell 150:1029–1041. https://doi.org/10.1016/j.cell.2012.06.050.
44. Selyunin AS, Sutton SE, Weigele BA, Reddick LE, Orchard RC, Bresson SM, Tomchick DR, Alto NM. 2011. The assembly of a GTPase-kinase signalling complex by a bacterial catalytic scaffold. Nature 469:107–111. https://doi.org/10.1038/nature09593.
45. Selyunin AS, Reddick LE, Weigele BA, Alto NM. 2014. Selective protection of an ARF1-GTP signaling axis by a bacterial scaffold induces bidirectional trafficking arrest. Cell Rep 6:878–891. https://doi.org/10.1016/j.celrep.2014.01.040.
46. Ho SN, Hunt HD, Horton RM, Pullen JK, Pease LR. 1989. Site-directed mutagenesis by overlap extension using the polymerase chain reaction. Gene 77:51–59. https://doi.org/10.1016/0378-1119(89)90358-2.
47. Edwards RA, Keller LH, Schifferli DM. 1998. Improved allelic exchange vectors and their use to analyze 987P fimbria gene expression. Gene 207:149–157. https://doi.org/10.1016/S0378-1119(97)00619-7.
48. Darfeuille-Michaud A, Neut C, Barnich N, Lederman E, Di Martino P, Desreumaux P, Gambiez L, Joly B, Cortot A, Colombel JF. 1998. Presence of adherent *Escherichia coli* strains in ileal mucosa of patients with Crohn's disease. Gastroenterology 115:1405–1413. https://doi.org/10.1016/S0016-5085(98)70019-8.
49. Gauthier A, Puente JL, Finlay BB. 2003. Secretin of the enteropathogenic *Escherichia coli* type III secretion system requires components of the type III apparatus for assembly and localization. Infect Immun 71:3310–3319. https://doi.org/10.1128/IAI.71.6.3310-3319.2003.
50. Warawa J, Finlay BB, Kenny B. 1999. Type III secretion-dependent hemolytic activity of enteropathogenic *Escherichia coli*. Infect Immun 67:5538–5540.
51. Kenny B, Jepson M. 2000. Targeting of an enteropathogenic *Escherichia coli* (EPEC) effector protein to host mitochondria. Cell Microbiol 2:579–590. https://doi.org/10.1046/j.1462-5822.2000.00082.x.
52. Valdivia RH, Falkow S. 1996. Bacterial genetics by flow cytometry: rapid isolation of *Salmonella typhimurium* acid-inducible promoters by differential fluorescence induction. Mol Microbiol 22:367–378. https://doi.org/10.1046/j.1365-2958.1996.00120.x.
53. Deng W, Puente JL, Gruenheid S, Li Y, Vallance BA, Vazquez A, Barba J, Ibarra JA, O'Donnell P, Metalnikov P, Ashman K, Lee S, Goode D, Pawson T, Finlay BB. 2004. Dissecting virulence: systematic and functional analyses of a pathogenicity island. Proc Natl Acad Sci U S A 101:3597–3602. https://doi.org/10.1073/pnas.0400326101.